IMPEDANCE MATRIX FORMALISM FOR THE SELF-CONSISTENT MODELING OF LOOP ANTENNAS IN THE ION CYCLOTRON FREQUENCY RANGE

M. Brambilla

IPP 5/45

March 1992

MAX-PLANCK-INSTITUT FÜR PLASMAPHYSIK

8046 GARCHING BEI MÜNCHEN

MAX-PLANCK-INSTITUT FÜR PLASMAPHYSIK

GARCHING BEI MÜNCHEN

IMPEDANCE MATRIX FORMALISM FOR THE SELF-CONSISTENT MODELING OF LOOP ANTENNAS IN THE ION CYCLOTRON FREQUENCY RANGE

M. Brambilla

IPP 5/45

March 1992

Die nachstehende Arbeit wurde im Rahmen des Vertrages zwischen dem Max-Planck-Institut für Plasmaphysik und der Europäischen Atomgemeinschaft über die Zusammenarbeit auf dem Gebiete der Plasmaphysik durchgeführt.

IMPEDANCE MATRIX FORMALISM FOR THE SELF–CONSISTENT MODELING OF LOOP ANTENNAS IN THE ION CYCLOTRON FREQUENCY RANGE

M. Brambilla

Max Planck Institute für Plasmaphysik
EURATOM Association
Fed. Rep. Germany

ABSTRACT

The technique of impedance and admittance matrices allows a simple and elegant solution of the problem of radiation from antennas of arbitrary shape and orientation in plane stratified geometry. The medium towards which the antenna radiates is completely characterised by the values of these matrices at its surface, which for a hot plasma in the IC frequency range we obtain numerically in the finite Larmor radius approximation. In vacuum, the wave admittance and impedance matrices obey simple transformation rules, which are used to solve the matching problem for arbitrary source currents.

Combined with the variational approach originally developed for the case of fast wave launching by K. Teilhaber and J. Jacquinot, this method allows the determination of the self–consistent current distribution in the antenna, its radiation resistance and its reactive impedance. The flexibility of the approach is illustrated by several examples, both without and with plasma loading. They include a discussion of the characteristics of the folded antenna which will be used for fast wave ICR heating in the ASDEX Upgrade tokamak, and of T–antennas for launching ion Bernstein waves near the first ion cyclotron harmonic.

This report gives several details of the theory which could not be included in the limited space available for publication: a proof of the variational principle, and its generalisation to the case of interacting antennas; a complete derivation and more explicit expressions for the transformation rules of the admittance and impedance matrices in vacuum; and the detailed procedure to solve the matching equations in the case of antennas with several layers of conductors (folded antennas).

1 – Introduction.

Antennas designed to launch h.f. waves in the ion cyclotron frequency domain into fusion–oriented magnetically confined plasmas usually consist of a set of conductors lying just outside the limiter or separatrix, fed by one or more a coaxial lines, and screened from the plasma by a Faraday shield. The simplest method to determine the loading resistance of such antennas consists in making a plausible guess on the current distribution $\vec{J}^a$ in the antenna conductors, and to evaluate the fields radiated by these currents, taking into account the appropriate boundary conditions at the wall, Faraday shield, and plasma edge. The loading resistance is then given by

$$R_a = \frac{\mathrm{Re} \int_A \vec{E}^*(\vec{r}) \cdot \vec{J}^a(\vec{r}) d\vec{r}}{I_A^2} \tag{1.1}$$

where the integral extends over the surface of the radiating elements, and I_A is the total current. This approach, known as the EMF method, has been pioneered by J. Adam[1] for fast wave launching. It has since been successfully developed to include an increasingly sophisticated description of the antenna, first in two–dimensions[2]–[3], then in fully tree–dimensional geometry[4]–[10]. More recently, it has been extended also to antennas designed to launch ion Bernstein waves[11]–[12].

Within the EMF model, it is possible to take into account feeders and shorts[5], and the Faraday screen is easily simulated as an infinite plane sheet ideally conducting along the blades, and perfectly transparent in the orthogonal direction. The model has also been extended to recessed antennas cased in a metallic box open towards the plasma[10] or between auxiliary limiters[13]. Nevertheless, it is rather difficult to take into account complicate passive elements, such as a discrete shield of finite extent: to model such components, ad–hoc approximations have been developed[14]–[17], based on the quasistatic approximation for the near field with only a crude model for the plasma.

Strictly speaking, moreover, the current distribution $\vec{J}^a(\vec{r})$ in the antenna is not known *a priori*, but should be evaluated selfconsistently, taking into account that the antenna conductors impose a metallic boundary condition on the tangential component of the electric field. This is particularly important when the frequency is relatively high, and for large devices, where the antenna is not necessarily electrically short. Although in some cases it is possible to find selfconsistent solutions directly[18]–[19], a more elegant and flexible method, based on the minimization of an appropriate functional[24], has been developed by Teilhaber and Jacquinot[20]–[21] and by Puri[22]–[23].

The variational approach was formulated in[20]–[23] for the case of fast wave coupled to a cold plasma. In this paper we generalise it to arbitrarily oriented antennas. This

generalisation is required for example to model Bernstein wave couplers[12], or to investigate the effects of misalignment of the antenna and Faraday screen with respect to magnetic field lines[25]. For this purpose, it is necessary in the vacuum layer to take into account both TE and TM modes, and in the plasma to solve wave equations including finite temperature effects. For the second task we have used the FELICE code, which integrates the finite Larmor radius wave equations[26] through the plasma cross–section in a plane–layered approximatrion to the real toroidal geometry. To solve Maxwell equations in vacuum with the required generality, on the other hand, we find it convenient to use the wave impedance matrix formalism. This method is of considerable interest in itself, and greatly simplifies the task of imposing boundary and matching conditions in the presence of arbitrary sources.

The plan of the paper is as follows. In section 2 we review the variational approach following closely Teilhaber and Jacquinot[20]. The next two sections are devoted to derive the relation between the currents in the antenna and the fields excited. This task is in principle the same as in the EMF approach; to deal conveniently with arbitrarily oriented antennas, however, we introduce in section 3 the impedance matrix formalism. A well–known advantage of this approach is that the medium towards which the antenna radiates is completely characterised by the values of this matrix at its surface, which we obtain for a hot plasma in the finite Larmor radius approximation from the FELICE code. In vacuum, the wave admittance and impedance matrices obey simple transformation rules, which are similar to the well–known ones for transmission lines. In section 4 we show that these transformation rules can be used to obtain an elegant solution of the problem of radiation from rather arbitrary *given* source currents, both without and with an ideal Faraday screen.

Once the fields radiated by given sources are known, the variational functional is easily constructed, and can be varied to determine the currents selfconsistently. A few examples of this procedure are presented in section 5. A natural way of specifying $\vec{J}^a$ is to regard the antenna conductors as finite pieces of transmission–line, with distributed inductance and capacity per unit length, L and C. In the EMF approach these quantities can be estimated from a simple quasistatic model[4], or measured experimentally. In the examples of section 5 we use the propagation constant along the antenna as variational parameter, and compare the results with an alternative variational procedure based on a Ritz expansion, also due to Teilhaber and Jacquinot[20].

Most of the applications presented in section 5 are confined to standard antennas with ideal Faraday shield. However, an advantage of the formalism introduced here is the fact that it can be easily generalised to more complicated situations. One example is

the evaluation of the characteristics of the ICRH antenna which will be used in ASDEX Upgrade[28], discussed in section 5.5. A 'naive' solution of the matching conditions for this two–layered antenna would be a very complicated task; once the procedure outlined in section 3 is implemented numerically, on the other hand, the problem is reduced to enter a few data for the description of the antenna geometry. The results compare very well with those obtained with a much more time–consuming Finite Element analysis[28].

Another situation in which the combination of the impedance matrix formalism with the variational approach of Teilhaber and Jacquinot yelds non–trivial results is for antennas designed to launch ion Bernstein waves (section 5.6). In this case we find that the selfconsistent current is appreciably influenced by the plasma, so that the loading resistance predicted by the EMF approach can be wrong by as much as a factor 2.

This report gives several details of the theory which could not be included in the limited space available for publication. The most important are: a proof of the variational principle and its generalisation to the case of several conductors; a complete derivation and more explicit expressions for the transformation rules of the admittance and impedance matrices in vacuum; and the details of the procedure to solve the matching equations in the case of antennas with several layers of conductors (folded antennas). Also, the examples are presented in some more details, including a short discussion of wave propagation and absorption in the plasma, which does not stricly belong to the antenna theory, but is useful to understand the loading results. In spite of the limited space available for the examples, we hope they will suffice to prove that the FELICE code combined with the antenna model developed in this work provides an excellent tool for the modeling of metallic antennas in the ion cyclotron frequency range.

2 – Variational formulation of the selfconsistent antenna problem.

2.1 – The complex impedance as variational functional. To formulate the selfconsistent antenna problem in variational form, we consider first for simplicity an antenna consisting of a single active element. The connection of the radiating conductor with its feeders can be idealised by an almost singular field applied by the power source in the plane of the wall (knife–edge model):

$$\vec{E}^{ext}(\vec{r}) = \delta(x+w)\left\{\Theta_F(y,z)\,\frac{V_F}{d_F}\right\}\vec{e}_x \tag{2.1}$$

where Θ_F is a step function with value unity in front of the feeder and zero elsewhere; V_F is the applied voltage, and d_F the width of the feeder (Θ_F/d_F can be replaced by

the appropriate δ–function in the limit $d_F \to 0$). By definition, the ratio of $V_F \delta_F$ to the total current through the feeder I_A is the complex antenna impedance Z_A:

$$V_F / d_F = Z_A I_A \tag{2.2}$$

Since

$$I_A = \int_A J_x^a(-w, y, z) \Theta_F(y, z)\, dy\, dz \tag{2.3}$$

where $\vec{J}^a(\vec{r})$ is the current density in the antenna, Eqs. (2.1) and (2.2) define a linear relation between $\vec{E}^{ext}$ and $\vec{J}^a$:

$$\begin{aligned} \vec{E}^{ext}(\vec{r}) &= Z_A \delta(x + w) \Theta_F(y, z) \int_A J_x^a(-w, y, z) \Theta_F(y, z)\, dy\, dz \\ &= -Z_A \underline{\underline{\mathcal{M}}} \cdot \vec{J}^a(\vec{r}) \end{aligned} \tag{2.4}$$

The field induced by the current flowing in the antenna, $\vec{E}_t^{ind}$, is also a linear functional of all currents in the antenna. In particular, we will denote its tangential component along the antenna conductor as

$$\vec{E}_t^{ind}(\vec{r}) = \underline{\underline{\mathcal{R}}}^a \cdot \vec{J}^a(\vec{r}) \tag{2.5}$$

Since the antenna is assumed to be a perfect conductor, we must have

$$\vec{E}_t^{ext}(\vec{r}) + \vec{E}_t^{ind}(\vec{r}) = 0 \qquad \vec{r} \text{ on } A \tag{2.6}$$

Using (2.4) and (2.5), we can rewrite this as an eigenvalue equation,

$$\underline{\underline{\mathcal{R}}}^a \cdot \vec{J}^a(\vec{r}) = Z_A \underline{\underline{\mathcal{M}}} \cdot \vec{J}^a(\vec{r}) \qquad \vec{r} \text{ on } A \tag{2.7}$$

from which a variational formulation is straightforwardly obtained. Multiplying both sides with an arbitrary current density $\vec{K}^a(\vec{r})$ and integrating over the antenna, we get

$$Z_A = \frac{1}{M} \int_A \vec{K}^{a*}(\vec{r}) \cdot \underline{\underline{\mathcal{R}}}^a \cdot \vec{J}^a(\vec{r}) d\vec{r} \tag{2.8}$$

with

$$M = \int_A \vec{K}^{a*}(\vec{r}) \cdot \underline{\underline{\mathcal{M}}} \cdot \vec{J}^a(\vec{r}) d\vec{r} = K_A^* I_A \tag{2.9}$$

where I_A, K_A are the total currents through the feeders associated with the distributions $\vec{J}^a(\vec{r})$ and $\vec{K}^a(\vec{r})$, respectively; the last equality follows immediately from Eqs. (2.1)–(2.3). If we consider a small variation in the current, we find that the corresponding change in Z_A is given by

$$\begin{aligned} \delta Z_A = \frac{1}{M} \Big\{ & \int_A \delta \vec{K}^{a*} \cdot \left(\underline{\underline{\mathcal{R}}}^a \cdot \vec{J}^a - Z_A \underline{\underline{\mathcal{M}}} \cdot \vec{J}^a \right) d\vec{r} \\ & + \int_A \delta \vec{J}^{a*} \cdot \left(\underline{\underline{\mathcal{R}}}^{a\dagger} \cdot \vec{K} - Z_A \underline{\underline{\mathcal{M}}}^\dagger \cdot \vec{K} \right) d\vec{r} \Big\} \end{aligned} \tag{2.10}$$

where $\underline{\underline{\mathcal{R}}}^{a\,\dagger}$ and $\underline{\underline{\mathcal{M}}}^{\dagger}$ are the Hermitean conjugate operators (actually, $\underline{\underline{\mathcal{M}}}^{\dagger} = \underline{\underline{\mathcal{M}}}$). Hence if $\vec{J}^a$ and $\vec{K}^a$ satisfy respectively (2.7) and its hermitean conjugate, δZ_A vanishes. Viceversa if we require $\delta Z_A = 0$, $\vec{J}^a$ and $\vec{K}^a$ will satisfy these equations.

The relation between this functional and the energy theorem (1.1) is obvious: if both $\vec{J}^a$ and $\vec{K}^a$ are identified with the actual current in the antenna, the real part of Z_A after the variation is performed gives the antenna resistance, and its imaginary part gives the reactive impedance. Loosely speaking, the selfconsistent current distribution in the antenna minimises the energy stored in the excited fields.

The operator $\underline{\underline{\mathcal{R}}}^a$ is explicitly obtained by solving the problem in the usual way, i.e. as if the antenna currents $\vec{J}^a(\vec{r})$ where known. As it is well–known, in the presence of plasma this solution is more easily obtained in Fourier space, using a plane–stratified approximation to the real geometry, and considering separately each Fourier component of fields and currents with given wavenumbers n_y and n_z in the ignorable coordinates y, z (cfr. next section). In Fourier space Eq. (2.5) can be rewritten

$$\vec{E}_t^a(n_y, n_z) = \underline{\underline{\mathcal{R}}}^a(n_y, n_z) \cdot \vec{J}^a(n_y, n_z) \tag{2.11}$$

where $\vec{E}_t^a$ is the value of the tangential component of the electric field amplitude in the plane of the antenna. Parseval theorem immediately gives the Fourier representation of the variational functional:

$$Z_A = \frac{4\pi^2 R_p r_p}{K_A^* I_A} \sum_{n_y} \sum_{n_z} \vec{K}^{a\,*}(n_y, n_z) \cdot \underline{\underline{\mathcal{R}}}^a(n_y, n_z) \cdot \vec{J}^a(n_y, n_z) \tag{2.12}$$

where R_p and r_p are the major and minor radius of the plasma. The variational procedure can be conveniently carried out directly in the Fourier representation.

2.2 – Ritz form of the variational equations. A particularly convenient implementation of the variational procedure, which does not require the explicit evaluation of the conjugate operator $\mathcal{R}^{a\,\dagger}$, was suggested in[20]. Again following closely Teilhaber and Jacquinot, we chose an appropriate set of functions $f_k(y, z)$ to expand

$$\vec{J}^a = \sum_k \alpha_k f_k(y, z) \vec{u}_A \qquad \vec{K}^{a\,*} = \sum_k \beta_k f_k(y, z) \vec{u}_A \tag{2.13}$$

where $\vec{u}_A$ is a unit vector orientated along the antenna. If $\bar{f}_k = f_k(y_F, z_F)$ are the values of the basis functions taken at the feeder position,

$$\sum_k \alpha_k \bar{f}_k = I_A \qquad \sum_k \beta_k \bar{f}_k = K_A^* \tag{2.14}$$

Eq. (2.12) then becomes

$$I_A K_A^* Z_A = \sum_l \sum_k \beta_l R_{lk} \alpha_k \tag{2.15}$$

with

$$\begin{aligned} R_{lk} &= \int_A f_l(\vec{r}) \left(\vec{u}_A \cdot \underline{\underline{\mathcal{R}}}^a \cdot \vec{u}_A\right) f_k(\vec{r})\, d\vec{r} = \\ & 4\pi R_p r_p \sum_{n_y} \sum_{n_z} f_l(n_y, n_z) \left(\vec{u}_A \cdot \underline{\underline{R}}^a(n_y, n_z) \cdot \vec{u}_A\right) f_k(n_y, n_z) \end{aligned} \tag{2.16}$$

where $f_k(n_y, n_z)$ is the Fourier transform of the function $f_k(y, z)$. In this representation the variational equations take the form of linear systems:

$$\bar{f}_l I_A Z_A = \sum_k R_{lk} \alpha_k \qquad \bar{f}_k K_A^* Z_A = \sum_l \beta_l R_{lk} \tag{2.17}$$

Introducing the inverse matrix R_{lk}^{-1}, we obtain

$$\alpha_k = Z_A I_A \sum_l R_{kl}^{-1} \bar{f}_l \qquad \beta_k = Z_A K_A^* \sum_l \bar{f}_l R_{lk}^{-1} \tag{2.18}$$

and substituting into either of (2.14)

$$Z_A = \left(\sum_k \sum_l \bar{f}_k R_{kl}^{-1} \bar{f}_l \right)^{-1} \tag{2.19}$$

The last two equations provide the explicit solution for both the eigenvalue Z_A and the current distribution $\vec{J}^a(x, y)$.

2.3 – Input and radiation resistance. Although in this section the 'knife–edge' field (2.1) has been for convenience identified with the 'feeder', it should be clear that this idealised source could be located at any point along the antenna; on the other hand the numerical value of Z_A depends on the position at which the total current I_A is evaluated. If the feeder proper is taken as reference, one obtains the so–called input impedance and resistance. In this work however we have found it preferable to define I_A as the peak current at shorts; as a consequence in the following all numerical values will refer to the loading (or radiation) impedance and resistance of the antenna. When more shorts are present (T–antennas, dipole antennas), to ensure that the numerator in Eq. (1.1) represents the total radiated power I_A must be the sum of all short currents, as if all conductors were in parallel seen from a common feeder.

2.4 – Generalisation to several conductors. An antenna consisting of two or more parallel conductors lying in the same plane can be treated as a single conductor by appropriately redefining the Fourier spectre $\vec{J}^a(n_y, n_z)$. In all other case the previous approach must be generalised to take explicitly into account mutual interactions between loops.

In the general case, Eq. (2.2) becomes

$$V_{F_q}/d_q = \sum_p Z_{qp} I_{A_p} \tag{2.20}$$

where indexes p, q have been introduced to distinguish the conductors. The matrix Z_{qp} must be symmetric, and has therefore generally $N_c(N_c+1)/2$ independent elements, where N_c is the number of conductors. The linear operator $\underline{\underline{\mathcal{M}}}_{qp}$ can be easily made explicit by generalising (2.4):

$$\underline{\underline{\mathcal{M}}}_{qp} \cdot \vec{J}^a_p(\vec{r}_q) = -\delta(x+w)\Theta_{F_q}(y_q, z_q) \int_{A_p} J^a_{p,x}(-w, y_p, z_p)\Theta_{F_p}(y_p, z_p)\, dy_p\, dz_p \tag{2.21}$$

while Eqs. (2.4) and (2.5) must be rewritten

$$\vec{E}^{ext}_q(\vec{r}_q) = -\sum_p Z_{qp}\, \underline{\underline{\mathcal{M}}}_{qp} \cdot \vec{J}^a_p(\vec{r}_q) \tag{2.22}$$

and

$$\vec{E}^{ind}_q(\vec{r}_q) = \underline{\underline{\mathcal{R}}}_{qp} \cdot \vec{J}^a_p \tag{2.23}$$

respectively. To obtain a representation of $\underline{\underline{\mathcal{R}}}_{qp}$ we use again the Fourier representation of currents and fields. Let

$$\vec{E}_p(n_y, n_z, x_q) = \underline{\underline{R}}_{pq}(n_y, n_z, x_q) \cdot \vec{J}_p(n_y, n_z) \tag{2.24}$$

be the Fourier transform of the field induced in the plane of conductor q by a current flowing in the p–th conductor, all other conductors being passive. Then we can write the required relation as

$$\vec{E}^{ind}_q(\vec{r}_q) = \frac{1}{4\pi^2 R_p r_p} \sum_{n_y} \sum_{n_z} e^{i(n_y y_q + n_z z_q)} \underline{\underline{R}}_p(n_y, n_z, x_q) \cdot \int_{A_p} \vec{J}^a_p(\vec{r}_p)\, e^{-i(n_y y_p + n_z z_p)} d\vec{r}_p \tag{2.25}$$

from which $\underline{\underline{\mathcal{R}}}_{qp}$ can be read directly.

As in the previous case, we must impose

$$\vec{E}^{ext}_q(\vec{r}_q) = \vec{E}^{ind}_q(\vec{r}_q) \tag{2.26}$$

for each q. Now if we multiply (2.23) with the current $\vec{K}_q^a$ flowing in the q–th conductor, integrate over all conductors, and sum over q, we obtain in a few elementary steps

$$\sum_q \sum_p K^*_{A_q} Z_{qp} I_{A_p} = 4\pi^2 R_p r_p \sum_q \sum_p \sum_{n_y} \sum_{n_z} \vec{K}^*_q(n_y, n_z) \cdot \underline{\underline{R}}_{qp}(n_y, n_z) \cdot \vec{J}_p(n_y, n_z) \tag{2.27}$$

A complete set of independent equations is obtained by varying the currents $\vec{K}^*_q(\vec{r}_q)$, keeping $K^*_{A_q}$ and one of the total currents I_{A_p} in turn constant, with all others equal to zero (only one of the two equations obtained by interchanging q and p needs to to be retained). Since the voltage applied to each conductor can be chosen independently, there are just $N_c(N_c+1)/2$ independent conditions, which fully determine the impedance matrix Z_{qp}. The symmetry of Z_{qp} is easily proved by interchanging the role of the test and actual currents, and using easily proved symmetries of $\underline{\underline{R}}_{pq}$. These results can be summarised by stating that the selfconsistent current distribution minimises all self and mutual energies, as one would expect.

3 – Solution of Maxwell Equations in Vacuum.

3.1 – Plane waves in vacuum. In large tokamaks, the dimensions of the antenna and of the near–field region are sufficiently small to justify solving the coupling problem in a plane–stratified geometry, in which all equilibrium gradients are assumed to be perpendicular to the the static magnetic field. We use Cartesian coordinates with x–axis along the gradients and z–axis along the static magnetic field, so that y and z correspond to the poloidal and toroidal direction in the tokamak. In this model y and z are both ignorable coordinates, so that we can represent the antenna currents and the excited fields as Fourier series, with wavenumbers k_y and k_z taking discrete values due to the double periodicity of the tokamak. As well–known, this decomposition is essential to simplify the solution of the wave equations within the plasma. In this section we consider the solution of Maxwell equations for the amplitudes $\vec{E}(k_y, k_z, x)$ and $\vec{B}(k_y, k_z, x)$ in a vacuum region free of sources.

In this simplified geometry the radial components E_x and B_x can be expressed algebraically in terms of the tangential ones (these denominations refer to the orientation with respect to magnetic surfaces). Moreover, once the appropriate jump conditions have been imposed on the tangential components at antenna conductors, those for E_x and B_x follow automatically, taking into account the continuity equation for the charge

on the conductors. It is therefore convenient to eliminate E_x and B_x from Maxwell equations, thereby obtaining for the tangential components the system:

$$\begin{aligned} \frac{1}{k_o}\frac{dE_y}{dx} &= i\left[(1-n_y^2)B_z + n_y n_z B_y\right] \\ \frac{1}{k_o}\frac{dE_z}{dx} &= -i\left[n_y n_z B_z + (1-n_z^2)B_y\right] \end{aligned} \tag{3.1a}$$

$$\begin{aligned} \frac{1}{k_o}\frac{dB_z}{dx} &= i\left[(1-n_z^2)E_y + n_y n_z E_z\right] \\ \frac{1}{k_o}\frac{dB_y}{dx} &= -i\left[n_y n_z E_y + (1-n_y^2)E_z\right] \end{aligned} \tag{3.1b}$$

where $k_o = \omega/c$ and $n_y = ck_y/\omega$, $n_z = ck_z/\omega$.

If either $n_y = 0$ or $n_z = 0$, these equations split into two independent set, the first for E_y and B_z only, the second for E_z and B_y only. The former are *transverse electric* (shortened TE), the second *transverse magnetic* (shortened TM) modes. When both n_y and n_z are different from zero, the solution is neither transverse electric nor transverse magnetic. These mixed modes are needed to be able to satisfy general boundary conditions, since strictly TE and TM modes alone do not form a *complete set* of solutions in the mathematical sense. It is nevertheless useful to regard the equations for E_y and B_z on the one hand, for E_z and B_y on the other, as two separate systems, although in general coupled to each other. In vacuum there is a complete symmetry between TE and TM modes, if the corresponding sets of variables are taken to be (E_y, B_z), $(E_z, -B_y)$, respectively. This symmetry moreover holds for any medium in which Onsager relations are satisfied: this is the case for a magnetised plasma if the z–axis is aligned with the static magnetic field.

The solution of Eqs. (3.1) is the superposition of two plane waves of the form

$$\vec{E}(n_y, n_z, x) = \sum\nolimits_{\pm} \vec{E}_{\pm} e^{\pm i k_x x} \qquad \vec{B}(n_y, n_z, x) = \sum\nolimits_{\pm} \vec{B}_{\pm} e^{\pm i k_x x} \tag{3.2}$$

where k_x must satisfy the vacuum dispersion relation $c^2k_x^2/\omega^2 + n_y^2 + n_z^2 = 1$; thus

$$\frac{c}{\omega}k_x = \begin{cases} n_x = \sqrt{1 - n_y^2 + n_z^2} & \text{if } n_y^2 + n_z^2 \le 1 \\ i\nu_x = i\sqrt{n_y^2 + n_z^2 - 1} & \text{if } n_y^2 + n_z^2 \ge 1 \end{cases} \tag{3.3}$$

With these definitions, the upper sign in (3.2) corresponds to a wave propagating in the positive direction, or evanescent towards the positive direction. To simplify notations, in the following we will measure lengths in units of c/ω, so that $k_o = \omega/c$ will disappear from the phase factors.

In slab geometry, a particular solution of Maxwell equations in vacuum is completely specified by the values of the four tangential components E_y^o, E_z^o, B_y^o, B_z^o at an arbitrary plane $x = x_o$; this solution can be written:

$$\begin{aligned} E_y &= E_y^o \cosh \nu_x (x - x_o) \\ &\quad + \frac{i}{\nu_x} \left[(1 - n_y^2) B_z^o + n_y n_z B_y^o \right] \sinh \nu_x (x - x_o) \\ E_z &= E_z^o \cosh \nu_x (x - x_o) \\ &\quad - \frac{i}{\nu_x} \left[n_y n_z B_z^o + (1 - n_z^2) B_y^o \right] \sinh \nu_x (x - x_o) \end{aligned} \tag{3.4a}$$

$$\begin{aligned} B_z &= B_z^o \cosh \nu_x (x - x_o) \\ &\quad + \frac{i}{\nu_x} \left[(1 - n_z^2) E_y^o + n_y n_z E_z^o \right] \sinh \nu_x (x - x_o) \\ B_y &= B_y^o \cosh \nu_x (x - x_o) \\ &\quad - \frac{i}{\nu_x} \left[n_y n_z E_y^o + (1 - n_y^2) E_z^o \right] \sinh \nu_x (x - x_o) \end{aligned} \tag{3.4b}$$

We have written these equations only for the case of evanescent waves, $n_y^2 + n_z^2 \geq 1$, since in the IC frequency domain the largest part of the launched spectrum satisfies this condition; to obtain the expressions valid for propagative waves it is sufficient to perform the substitution $\nu_x \to -in_x$, so that hyperbolic functions go over into circular functions.

3.2 – The wave admittance and impedance matrices. Although the general solution of Maxwell equations depends on four arbitrary constants (e.g. the four constants $E_\pm$, $B_\pm$ in Eqs. (3.2), or the four values E_y^o, E_z^o, B_y^o, B_z^o at $x = x_o$), it is well known that physical solutions depend only on two independent constants. A field excited by a localised source cannot contain waves propagating towards the source, or growing exponentially away from the source: causality eliminates half of the degrees of freedom of the complete solution sketched in the previous paragraph.

A useful and general way of specifying the physically admissible solutions is in term of wave impedances or admittances. Suppose that by solving the appropriate set of Maxwell equations in the region $x \geq x_o$ taking into account all appropriate conditions (causality, matching at discontinuities, reflection from metallic walls, etc.; it is only assumed that this region does not contain sources), we have determined the set of physical solutions to the right of the plane $x = x_o$. For these solutions, two of the four constants E_y^o, E_z^o, B_y^o, B_z^o must be expressible in terms of the other two; moreover this relation must be linear, since Maxwell equations are linear and any linear combination of physical solutions must also be physically acceptable.

Such a relation is best expressed in matrix form. For this purpose, it is convenient to define the 'tangential field vectors' in a way which takes into account the symmetry between TE and TM modes mentioned above, namely

$$\begin{aligned} \vec{E}_t &= \vec{E} - (\vec{u}_x \cdot \vec{E})\,\vec{u}_x = E_y\vec{u}_y + E_z\vec{u}_z \\ \vec{B}_t &= -\vec{u}_x \times \vec{B} = B_z\vec{u}_y - B_y\vec{u}_z \end{aligned} \tag{3.5}$$

For physically acceptable waves the values of these vectors on the reference plane $x = x_o$ must be linearly related to each other:

$$\vec{B}_t^o = \underline{\underline{Y}}^o \cdot \vec{E}_t^o \qquad\qquad \vec{E}_t^o = \underline{\underline{Z}}^o \cdot \vec{B}_t^o \tag{3.6}$$

The 2×2 matrices Y_{ij}^o and Z_{ij}^o (whose elements are functions of n_y and n_z) are called respectively the surface admittance and impedance matrix of the half space $x \geq x_o$. By definition they are each the inverse of the other:

$$\underline{\underline{Z}}^o = (\underline{\underline{Y}}^o)^{-1} \tag{3.7}$$

It is also easily seen that whenever the symmetry mentioned above between TE and TM modes holds, the matrices $\underline{\underline{Y}}^o$ and $\underline{\underline{Z}}^o$ are symmetric,

$$Y_{21}^o = Y_{12}^o \qquad\qquad Z_{21}^o = Z_{12}^o \tag{3.8}$$

It is worth noting here that notations are greatly simplified by the fact that in Gauss cgs units $\underline{\underline{Y}}^o$ and $\underline{\underline{Z}}^o$ are dimensionless. The transition to MKSA units is however quite simple: it is sufficient to replace $\vec{B}$ by $\vec{H}$ throughout, omit the factor $4\pi/c$ multiplying the current density, and define the admittance and impedance matrices in the MKSA system in terms of those used here as

$$\underline{\underline{Z}}^{MKSA} = \sqrt{\frac{\mu_o}{\epsilon_o}}\,\underline{\underline{Z}}^o \qquad\qquad \underline{\underline{Y}}^{MKSA} = \sqrt{\frac{\epsilon_o}{\mu_o}}\,\underline{\underline{Y}}^o \tag{3.9}$$

where ϵ_o, μ_o are the electric and magnetic permeability of vacuum, respectively, and $\sqrt{\mu_o/\epsilon_o} = 120\pi$ Ohms.

The surface impedance or admittance matrices completely characterise the half–space $x \geq x_o$ from the point of view of wave propagation: if they are known, Maxwell equations with given sources to the left of this plane can be completely solved without further information about the nature of the medium to the right. This circumstance allows to split the antenna problem into two conceptually and practically separate parts: the determination of the surface impedance matrix of the plasma for all values of n_y, n_z, on the one hand, and the solution of the appropriate boundary conditions in vacuum

(taking into account source conductors and the presence of metallic walls) on the other hand. In particular, the power flux per unit area through the reference plane $x = x_o$ can be expressed in terms of these matrices and the amplitudes of either $\vec{E}_t^o$ or $\vec{B}_y^o$ only. In vacuum, this flux is given by the x component of the Poynting vector; using (3.6) we get

$$P_x(n_y, n_z) = \frac{c}{8\pi}\mathrm{Re}\left(\vec{E}_t^* \cdot \underline{\underline{Y}}^o \cdot \vec{E}_t\right) = \frac{c}{8\pi}\mathrm{Re}\left(\vec{B}_t^* \cdot \underline{\underline{Z}}^o \cdot \vec{B}_t\right) \tag{3.10}$$

3.3 – Examples: a) Vacuum half–space. In the simplest case the half–space $x \geq x_o$ is empty, i.e. the antenna radiates in vacuum. Then the solution satisfying causality consists of plane waves propagating towards positive infinity, or evanescent in the positive direction. Substituting this Ansatz into Eqs. (3.1) we immediately obtain

$$\begin{aligned} \underline{\underline{Y}}^o = \underline{\underline{N}} &= \frac{1}{n_x}\begin{pmatrix} (1-n_z^2) & n_y n_z \\ n_y n_z & (1-n_y^2) \end{pmatrix} \\ \underline{\underline{Z}}^o = \underline{\underline{M}} &= \frac{1}{n_x}\begin{pmatrix} (1-n_y^2) & -n_y n_z \\ -n_y n_z & (1-n_z^2) \end{pmatrix} \end{aligned} \tag{3.11a}$$

if $n_y^2 + n_z^2 \leq 1$, and

$$\begin{aligned} \underline{\underline{Y}}^o = \underline{\underline{N}} &= -\frac{i}{\nu_x}\begin{pmatrix} (1-n_z^2) & n_y n_z \\ n_y n_z & (1-n_y^2) \end{pmatrix} \\ \underline{\underline{Z}}^o = \underline{\underline{M}} &= -\frac{i}{\nu_x}\begin{pmatrix} (1-n_y^2) & -n_y n_z \\ -n_y n_z & (1-n_z^2) \end{pmatrix} \end{aligned} \tag{3.11b}$$

if $n_y^2 + n_z^2 > 1$. It is immediate to recognise that $\underline{\underline{M}}$ and $\underline{\underline{N}}$ are the inverse of each other, and that

$$\det(\underline{\underline{M}}) = \det(\underline{\underline{N}}) = 1 \tag{3.12}$$

Moreover the elements of $\underline{\underline{M}}$ and $\underline{\underline{N}}$ are purely real if $n_y^2 + n_z^2 \leq 1$, and purely imaginary in the opposite case. Substituting into (10) it is seen that only propagating waves can transport power through the $x = 0$ plane, as one would expect.

b) Vacuum slab terminated by a perfectly conducting wall. Another interesting case is when a perfectly conducting wall is located at a distance x_w from the reference plane $x = x_o$. At such a wall the tangential components of $\vec{E}$ must vanish; imposing this condition on the general solution (3.4) and eliminating the values of the tangential components of $\vec{B}$ at the metallic plate, we find (for brevity we write again only the expressions valid for $n_y^2 + n_z^2 > 1$)

$$\begin{aligned} \underline{\underline{Y}}^o &= -\frac{\cosh \nu_x (x_o - x_w)}{\sinh \nu_x (x_o - x_w)} \underline{\underline{N}} \\ \underline{\underline{Z}}^o &= -\frac{\sinh \nu_x (x_o - x_w)}{\cosh \nu_x (x_o - x_w)} \underline{\underline{M}} \end{aligned} \tag{3.13}$$

In particular, the surface impedance at a perfectly conducting wall vanishes, hence its inverse does not exist (its elements are formally infinite).

Since the elements of the matrices (3.13) are purely imaginary for both propagative and evanescent waves, it follows that no power can be transmitted through a plane facing a ideally conducting wall, as one would expect. It would however be wrong to conclude that the radiation resistance of an antenna facing such a wall vanishes: if the system is infinite in at least one direction, power can be radiated into modes guided along the wall. This manifests itself in the divergences of (3.13) for the appropriate real values of k_x: the radiation resistance in this case can be evaluated by adding an infinitesimal amount of dissipation.

c) Impedance and admittance matrices of a resistive wall. The surface impedance at a resistive wall is

$$\begin{aligned} \underline{\underline{Y}}^w = \underline{\underline{Q}} &= \frac{\hat{\sigma}}{\nu_\sigma} \begin{pmatrix} 1 + i\frac{n_z^2}{\hat{\sigma}} & -i\frac{n_y n_z}{\hat{\sigma}} \\ -i\frac{n_y n_z}{\hat{\sigma}} & 1 + i\frac{n_y^2}{\hat{\sigma}} \end{pmatrix} \\ \underline{\underline{Z}}^w = \underline{\underline{P}} &= -\frac{i}{\nu_\sigma} \begin{pmatrix} 1 + i\frac{n_y^2}{\hat{\sigma}} & i\frac{n_y n_z}{\hat{\sigma}} \\ i\frac{n_y n_z}{\hat{\sigma}} & 1 + i\frac{n_z^2}{\hat{\sigma}} \end{pmatrix} \end{aligned} \tag{3.14}$$

where $i\hat{\sigma} = 1 + (4\pi i/\omega)\sigma \simeq i(4\pi\sigma/\omega)$ and $\nu_\sigma^2 = n_y^2 + n_z^2 - i\hat{\sigma}$ (in MKSA units, replace $4\pi\sigma/\omega$ by $\sigma/\omega\epsilon_o$).

d) Plasma filled half–space. If the half–space $x > 0$ is filled with a material medium, the evaluation of the wave impedance or admittance matrices at $x = 0$ requires the knowledge of two linearly independent solutions of Maxwell equations in such medium,

satisfying the appropriate conditions either at infinity if the medium is unbounded to the right, or at a metallic wall if it is bounded. From the values of the tangential fields at $x = 0$ one obtains a linear system for the components of $\underline{\underline{Y}}^o$ (or $\underline{\underline{Z}}^o$); the linear independence of the two solutions guarantees that this system can be inverted.

In the case of a half–space filled with a non–homogeneous plasma, Maxwell equations can often be solved only numerically, and no generally useful analytic formula can be given for $\underline{\underline{Y}}^o$ or $\underline{\underline{Z}}^o$. Here we will only comment on a circumstance which makes a plasma a particularly complicated medium also from this point of view.

The procedure just outlined for the evaluation of the surface wave impedances is straightforward in the cold plasma limit, but a difficulty arises when finite temperature effects are taken into account. A hot plasma supports three characteristic waves, namely the two cold waves, and a pressure–driven wave (sometimes even a fourth eigenwave exists in the domain of higher order ion or electron Bernstein waves, but under realistic conditions this wave is unphysical near the plasma edge). The existence of three independent solutions satisfying causality makes the system for $\underline{\underline{Y}}^o$ underdetermined; this situation is not altered by the fact that at least one of the characteristic waves, namely the shear magnetosonic mode, is often strongly evanescent near the plasma edge in the ion frequency domain.

The paradox is easily resolved, however, by noting that in a hot plasma an additional condition must be satisfied at the plasma–vacuum boundary. When the plasma is described in the finite Larmor radius approximation, the required additional condition at the vacuum–plasma interface has been shown to follow automatically from the differential wave equations[12], [26]. The existence of such a condition is a consequence of the requirement that the power flux at the interface must be continuous. Indeed, the continuity of the tangential components of the fields, $\vec{E}_t$ and $\vec{B}_t$, at $x = 0$ guarantees the continuity of the radial component of the Poynting vector, i.e. of the 'elecromagnetic' part of the power flux through the plasma boundary. Hence the 'kinetic' part of the power flux, which exists in a hot plasma as a consequence of spatial dispersion[27], must vanish at the plasma edge. When this condition is taken into account the univocity of $\underline{\underline{Y}}^o$ is guaranteed.

3.4 – The scattering problem. The simplest application of the matrix formalism is to evaluate the reflection of a plane wave incident from vacuum on the plane $x = x_o$. The total field for $x < x_o$ can be written in terms of the amplitude of the incident wace as

$$\begin{aligned} \vec{E}_t(x) &= \left(e^{ik_x(x-x_o)} + \underline{\underline{\rho}}\, e^{-ik_x(x-x_o)}\right) \cdot \vec{E}_t^i \\ \vec{B}_t(x) &= \underline{\underline{N}} \cdot \left(e^{ik_x(x-x_o)} - \underline{\underline{\rho}}\, e^{-ik_x(x-x_o)}\right) \cdot \vec{E}_t^i \end{aligned} \tag{3.15}$$

where we have exploited the fact that the vacuum admittance matrix for the reflected wave is $-\underline{\underline{N}}$. Specialising this to the plane $x = x_o$ and comparing with the definitions (3.6), one easily gets the reflection matrix $\underline{\underline{\rho}}$ in terms of $\underline{\underline{Z}}^o$ or $\underline{\underline{Y}}^o$:

$$\underline{\underline{\rho}} = -\left(\underline{\underline{I}} + \underline{\underline{Z}}^o \cdot \underline{\underline{N}}\right)^{-1} \cdot \left(\underline{\underline{I}} - \underline{\underline{Z}}^o \cdot \underline{\underline{N}}\right) = -\left(\underline{\underline{I}} + \underline{\underline{M}} \cdot \underline{\underline{Y}}^o\right)^{-1} \cdot \left(\underline{\underline{I}} - \underline{\underline{M}} \cdot \underline{\underline{Y}}^o\right) \tag{3.16}$$

This example illustrates well the complete characterisation of the half–space $x \geq x_o$ by the admittance and impedance matrices of its surface.

3.5 – Transformation of the wave admittance and impedance matrices. If the surface admittance or impedance matrix is known at $x = x_o$, Eqs. (3.4) can be used to evaluate them at any other point x in vacuum. To obtain the explicit transformation formulae, it is useful first to rewrite these equations compactly as

$$\begin{aligned} \vec{E}_t(x) &= \cosh \nu_x(x - x_o) \left\{\vec{E}_t^o - \nu_x \tilde{T}_o \underline{\underline{M}} \cdot \vec{B}_t^o\right\} \\ \vec{B}_t(x) &= \cosh \nu_x(x - x_o) \left\{\vec{B}_t^o - \nu_x \tilde{T}_o \underline{\underline{N}} \cdot \vec{E}_t^o\right\} \end{aligned} \tag{3.17}$$

where $\vec{n}_t = n_y \vec{u}_y + n_z \vec{u}_z$, and we have defined the real function $\tilde{T}_o = \tilde{T}(n_y, n_z; x - x_o)$

$$\tilde{T}(n_y, n_z; x) = \begin{cases} \tan(n_x x)/n_x & \text{if } n_y^2 + n_z^2 \leq 1 \\ \tanh(\nu_x x)/\nu_x & \text{if } n_y^2 + n_z^2 > 1 \end{cases} \tag{3.18}$$

As a first step, we use Eqs. (3.6) to eliminate two of the four constants from Eqs. (3.17). This can be done in two ways, namely in favor of $\vec{E}_t^o$:

$$\begin{aligned} \vec{E}_t &= \cosh \nu_x(x - x_o)\, \underline{\underline{\Lambda}}^o \cdot \vec{E}_t^o \\ \vec{B}_t &= \cosh \nu_x(x - x_o)\, \underline{\underline{\Gamma}}^o \cdot \vec{E}_t^o \end{aligned} \tag{3.19a}$$

where

$$\begin{aligned} \underline{\underline{\Lambda}}^o &= \underline{\underline{I}} - \nu_x \tilde{T}_o \underline{\underline{M}} \cdot \underline{\underline{Y}}^o \\ \underline{\underline{\Gamma}}^o &= \underline{\underline{Y}}^o - \nu_x \tilde{T}_o \underline{\underline{N}} \end{aligned} \tag{3.20a}$$

or in favor of $\vec{B}_t^o$:

$$\begin{aligned}\vec{E}_t &= \cosh \nu_x (x - x_o)\, \underline{\underline{L}}^o \cdot \vec{B}_t^o \\ \vec{B}_t &= \cosh \nu_x (x - x_o)\, \underline{\underline{V}}^o \cdot \vec{B}_t^o\end{aligned} \tag{3.19b}$$

where

$$\begin{aligned}\underline{\underline{L}}^o &= \underline{\underline{Z}}^o - \nu_x \tilde{T}_o \underline{\underline{M}} \\ \underline{\underline{V}}^o &= \underline{\underline{I}} \; - \nu_x \tilde{T}_o \underline{\underline{N}} \cdot \underline{\underline{Z}}^o\end{aligned} \tag{3.20b}$$

From these equations it is immediate to obtain the admittance and impedance matrices at the plane x in the form:

$$\begin{aligned}\underline{\underline{Y}} &= \underline{\underline{\Gamma}}^o \cdot (\underline{\underline{\Lambda}}^o)^{-1} = \underline{\underline{V}}^o \cdot (\underline{\underline{L}}^o)^{-1} \\ \underline{\underline{Z}} &= \underline{\underline{L}}^o \cdot (\underline{\underline{V}}^o)^{-1} = \underline{\underline{\Lambda}}^o \cdot (\underline{\underline{\Gamma}}^o)^{-1}\end{aligned} \tag{3.21}$$

or more explicitly

$$\begin{aligned}\underline{\underline{Y}} &= \left(\underline{\underline{Y}}^o - \nu_x \tilde{T}(x - x_o)\underline{\underline{N}}\right) \cdot \left(\underline{\underline{I}} - \nu_x \tilde{T}(x - x_o)\underline{\underline{M}} \cdot \underline{\underline{Y}}^o\right)^{-1} \\ &= \left(\underline{\underline{I}} - \nu_x \tilde{T}(x - x_o)\underline{\underline{N}} \cdot \underline{\underline{Z}}^o\right) \cdot \left(\underline{\underline{Z}}^o - \nu_x \tilde{T}(x - x_o)\underline{\underline{M}}\right)^{-1} \\ \underline{\underline{Z}} &= \left(\underline{\underline{Z}}^o - \nu_x \tilde{T}(x - x_o)\underline{\underline{M}}\right) \cdot \left(\underline{\underline{I}} - \nu_x \tilde{T}(x - x_o)\underline{\underline{N}} \cdot \underline{\underline{Z}}^o\right)^{-1} \\ &= \left(\underline{\underline{I}} - \nu_x \tilde{T}(x - x_o)\underline{\underline{M}} \cdot \underline{\underline{Y}}^o\right) \cdot \left(\underline{\underline{Y}}^o - \nu_x \tilde{T}(x - x_o)\underline{\underline{N}}\right)^{-1}\end{aligned} \tag{3.22}$$

Elementary identities for 2×2 matrices give

$$\begin{aligned}\det(\underline{\underline{\Lambda}}^o) &= 1 - \nu_x \tilde{T}_o \,\mathrm{Tr}\,(\underline{\underline{M}} \cdot \underline{\underline{Y}}^o) + \nu_x^2 \tilde{T}_o^2 \det(\underline{\underline{Y}}^o) \\ \det(\underline{\underline{V}}^o) &= 1 - \nu_x \tilde{T}_o \,\mathrm{Tr}\,(\underline{\underline{N}} \cdot \underline{\underline{Z}}^o) + \nu_x^2 \tilde{T}_o^2 \det(\underline{\underline{Z}}^o)\end{aligned} \tag{3.23}$$

and

$$\begin{aligned}(\underline{\underline{\Lambda}}^o)^{-1} &= \frac{1}{\det(\underline{\underline{\Lambda}}^o)} \left(\underline{\underline{I}} - \nu_x \tilde{T}_o \det(\underline{\underline{Y}}^o)\underline{\underline{Z}}^o \cdot \underline{\underline{N}}\right) \\ (\underline{\underline{V}}^o)^{-1} &= \frac{1}{\det(\underline{\underline{V}}^o)} \left(\underline{\underline{I}} - \nu_x \tilde{T}_o \det(\underline{\underline{Z}}^o)\underline{\underline{Y}}^o \cdot \underline{\underline{M}}\right)\end{aligned} \tag{3.24}$$

With the help of these results and some straightforward algebra we finally obtain:

$$\begin{aligned}\underline{\underline{Y}} &= \frac{(1 - \nu_x^2 \tilde{T}_o^2)}{\det(\underline{\underline{\Lambda}}^o)} \left\{\underline{\underline{Y}}^o - \nu_x \tilde{T}_o \det(\underline{\underline{Y}}^o)\,\underline{\underline{N}}\right\} - \nu_x \tilde{T}_o \underline{\underline{N}} \\ \underline{\underline{Z}} &= \frac{(1 - \nu_x^2 \tilde{T}_o^2)}{\det(\underline{\underline{V}}^o)} \left\{\underline{\underline{Z}}^o - \nu_x \tilde{T}_o \det(\underline{\underline{Z}}^o)\,\underline{\underline{M}}\right\} - \nu_x \tilde{T}_o \underline{\underline{M}}\end{aligned} \tag{3.25}$$

Here $\mathrm{Tr}\,(\underline{\underline{M}} \cdot \underline{\underline{Y}}^o)$ and $\mathrm{Tr}\,(\underline{\underline{N}} \cdot \underline{\underline{Z}}^o)$ are the traces of the matrices $\underline{\underline{M}} \cdot \underline{\underline{Y}}^o$ and $\underline{\underline{N}} \cdot \underline{\underline{Z}}^o$, respectively:

$$\begin{aligned} \mathrm{Tr}\,(\underline{\underline{M}} \cdot \underline{\underline{Y}}^o) &= -\frac{i}{\nu_x}\left\{(1-n_y^2)Y_{11}^o + (1-n_z^2)Y_{22}^o - n_y n_z\,(Y_{12}^o + Y_{21}^o)\right\} \\ \mathrm{Tr}\,(\underline{\underline{N}} \cdot \underline{\underline{Z}}^o) &= -\frac{i}{\nu_x}\left\{(1-n_z^2)Z_{11}^o + (1-n_y^2)Z_{22}^o + n_y n_z\,(Z_{12}^o + Z_{21}^o)\right\} \end{aligned} \tag{3.26}$$

(note also that $1 - \nu_x^2 \tilde{T}_o^2 = \cosh^{-2} \nu_x (x - x_o)$).

It is immediately evident from Eqs. (3.22) that $\underline{\underline{Y}}$ and $\underline{\underline{Z}}$ are again the inverse of each other, as they should, and are symmetric if $\underline{\underline{Y}}^o$ and $\underline{\underline{Y}}^o$ are: in other words, Eqs. (3.7) and (3.8) hold at every point x. More generally, it is clear that the transformations (3.22) constitute a group. Although this statement is self–evident, its proof is somewhat involved, and will be omitted.

On the other hand a few lines of algebra allow to check that the vacuum admittance and impedance matrices, $\underline{\underline{N}}$ and $\underline{\underline{M}}$, are *invariant* under the transformations (3.22), as indeed they should. Similarly, the admittance and impedance matrices of a vacuum slab terminated by a perfectly conducting wall are *form–invariant*, i.e. when Eqs. (3.22) are applied to the matrices (3.13), they amount to the appropriate shift of the argument $x - x_w$ of the coefficients. Finally, the radial component of the Poynting vector can be written in the form (3.10) at any plane x. It is somewhat more complicated, but still straightforward, to prove that $P_x(x)$ also maintains the same numerical value when the impedance and transmittance matrices at x are obtained from those at the reference plane x_o using Eqs. (3.22). This of course reflects energy conservation in vacuum.

4. – The field radiated by given currents.

4.1 – Effect of feeder currents. If radial currents J_x are present, Eqs. (3.1) for the tangential fields, in vector dimensionless notations, become[5]:

$$\begin{aligned} \frac{d\vec{E}_t}{dx} &= -\nu_x \underline{\underline{M}} \cdot \left(\vec{B}_t + \frac{i}{\nu_x}\vec{J}_F\right) \\ \frac{d\vec{B}_t}{dx} &= -\nu_x \underline{\underline{N}} \cdot \vec{E}_t \end{aligned} \tag{4.1}$$

where for convenience we have abbreviated

$$\vec{J}_F(n_y, n_z) = \frac{4\pi}{c} J_x(n_y, n_z) \left(\frac{n_y}{\nu_x}\vec{u}_y + \frac{n_z}{\nu_x}\vec{u}_z\right) \tag{4.2}$$

and we have used the identities

$$\underline{\underline{M}} \cdot \vec{J}_F = i\nu_x \vec{J}_F \qquad\qquad \underline{\underline{N}} \cdot \vec{J}_F = -\frac{i}{\nu_x}\vec{J}_F \tag{4.3}$$

A forced solution of these equations can be immediately written if we assume for simplicity that J_x does not depend on x, as justified by the fact that radial conductors are always electrically short:

$$\vec{E}_t^f = 0 \qquad\qquad \vec{B}_t^f = -\frac{i}{\nu_x}\vec{J}_F \tag{4.4}$$

Combining it with the general solution of the homogeneous equations, the solution which satisfy $\vec{E}_t = \vec{E}_t^o$, $\vec{B}_t = \vec{B}_t^o$ at the reference plane $x = x_o$ within the layer (generalising Eqs. (3.4)) can be written

$$\begin{aligned} \vec{E}_t &= \cosh \nu_x (x - x_o) \left\{ \vec{E}_t^o - \nu_x \tilde{T}_o \underline{\underline{M}} \cdot \left(\vec{B}_t^o + \frac{i}{\nu_x}\vec{J}_F \right) \right\} \\ \vec{B}_t + \frac{i}{\nu_x}\vec{J}_F &= \cosh \nu_x (x - x_o) \left\{ \left(\vec{B}_t^o + \frac{i}{\nu_x}\vec{J}_F \right) - \nu_x \tilde{T}_o \underline{\underline{N}} \cdot \vec{E}_t^o \right\} \end{aligned} \tag{4.5}$$

In the presence of radial currents the form of these equations suggests to define the impedance and admittance matrices as relations between $\vec{E}_t$ and $\vec{B}_t + (i/\nu_x)\vec{J}_F$, rather than $\vec{B}_t$ alone. The transformation rules for $\underline{\underline{Z}}$ and $\underline{\underline{Y}}$ hold without change, but additional terms linear in $\vec{J}_F$ generally arise if the radial currents exist only in a finite layer. It is easily seen however that these terms vanish identically if this layer is bounded on one side by an ideally conducting wall.

4.2 – Matching at main conductors. Let the vacuum region between vessel and plasma be divided in N_c layers by the antenna conductors located in the planes $x = -a_k$ (the plasma surface is at $x = 0$, and the wall at $x = -w$. In each layer $-a_k \le x < -a_{k+1}$, and for each n_y and n_z, the field can be written in the form (4.5), which depends linearly on two unknown coefficients. They must be determined by imposing the matching conditions across the planes $x = -a_k$:

$$\left[\vec{E}_t\right]_{a_k} = 0 \qquad\qquad \left[\vec{B}_t\right]_{a_k} = -\vec{J}_t^{a_k}(n_y, n_z) \tag{4.6}$$

where brackets denote the jump across the $x = -a_k$ plane, and a factor $4\pi/c$ is again included for simplicitly in the definition of $\vec{J}_t^{a_k}(n_y, n_z)$. The simple but somewhat unusual form of the jump condition for the wave magnetic field follows from the definition (3.5) of $\vec{B}_t$.

If the wave admittance $\underline{\underline{Y}}_w$ at the wall $x = -w$ to the left, and $\underline{\underline{Y}}_p$ at the plasma edge $x = 0$ to the right of all conductors are known, the number of conditions equals the number of unknowns, so that the problem is well posed. The task of actually solving it is made surprisingly simple by the formalism developed in the previous section. The elimination of the unknown coefficients can be done in several ways; the most convenient is perhaps to start from the inner set of conductors, and work out towards the plasma edge. Usually the wall is assumed to be a perfect conductor; we will not restrict the formalism to this case for the moment, however, so that generalisations could be easily made, for example to take into account the finite resistivity of the wall.

1) To obtain the fields $\vec{E}_t^{a_1}$ and $\vec{B}_t^{a_1^-}$ on the side of the inner conductor facing the wall, we can use Eq. (4.5), written with $x_o = -w$, $x = -a_1$. Taking into account that at the wall we have by definition $\vec{B}_t^w = \underline{\underline{Y}}_w \cdot \vec{E}_t^w$, we obtain

$$\begin{aligned} \vec{E}_t^{a_1} &= \cosh \nu_x(w - a_1) \left\{ \underline{\underline{\Lambda}}_w^{a_1} \cdot \vec{E}_t^w - \nu_x \tilde{T}(w - a_1) \underline{\underline{M}} \cdot \left(\frac{i}{\nu_x} \vec{J}_{\Sigma F}^1 \right) \right\} \\ \vec{B}_t^{a_1^-} &+ \frac{i}{\nu_x} \vec{J}_{\Sigma F}^1 = \cosh \nu_x(w - a_1) \left\{ \underline{\underline{\Gamma}}_w^{a_1} \cdot \vec{E}_t^w + \frac{i}{\nu_x} \vec{J}_{\Sigma F}^1 \right\} \end{aligned} \tag{4.7}$$

with

$$\begin{aligned} \underline{\underline{\Lambda}}_w^{a_1} &= \underline{\underline{I}} - \nu_x \tilde{T}(w - a_1) \underline{\underline{M}} \cdot \underline{\underline{Y}}_w \\ \underline{\underline{\Gamma}}_w^{a_1} &= \underline{\underline{Y}}_w - \nu_x \tilde{T}(w - a_1) \underline{\underline{N}} \end{aligned} \tag{4.8}$$

and we have introduced the notation

$$\vec{J}_{\Sigma F}^j = \sum_{k=j}^{N} \vec{J}_F^{a_k} \tag{4.9}$$

for all radial currents in the layer behind the (j)–th conductor. Eliminating $\vec{E}_t^w$ between the two equations (4.7) we find

$$\vec{B}_t^{a_1^-} + \frac{i}{\nu_x} \vec{J}_{\Sigma F}^1 = \underline{\underline{Y}}_w^{a_1} \cdot \vec{E}_t^{a_1} - \vec{K}^{a_1} \tag{4.10}$$

Here, according to the rules of section (3.4), $\underline{\underline{Y}}_w^{a_1} = \underline{\underline{\Gamma}}_w^{a_1} \cdot (\underline{\underline{\Lambda}}_w^{a_1})^{-1}$ is just the admittance matrix of the wall seen from the plane $x = a_1$, and we have put

$$\vec{K}^{a_1} = -\frac{i}{\nu_x} \cosh \nu_x(w - a_1) \left\{ \underline{\underline{I}} + \nu_x \tilde{T}(w - a_1) \underline{\underline{Y}}_w^{a_1} \cdot \underline{\underline{M}} \right\} \cdot J_{\Sigma F}^1 \tag{4.11}$$

Now according to Eq. (4.6) $\vec{B}_t^{a_1^+} = \vec{B}_t^{a_1^-} - \vec{J}_t^{a_1}$; we thus get an equation for the fields on the outer side of this plane,

$$\vec{B}_t^{a_1^+} + \frac{i}{\nu_x} \vec{J}_{\Sigma F}^2 = \underline{\underline{Y}}_w^{a_1} \cdot \vec{E}_t^{a_1} - \left(\vec{J}_{eff}^{a_1} + \vec{K}^{a_1} \right) \tag{4.12}$$

where we have defined the 'effective' current of the j–conductor,

$$\vec{J}_{eff}^{a_j} = \vec{J}_t^{a_j} + \frac{i}{\nu_x}\vec{J}_F^{a_j} \tag{4.13}$$

and the sum on the feeders extends now only to those of outer conductors.

2) Suppose next that the elimination procedure has been carried out till the outer side of the conductors in the plane $x = -a_{j-1}$, at which therefore a condition of the form (4.12) will have been obtained,

$$\vec{B}_t^{a_{j-1}^+} + \frac{i}{\nu_x}\vec{J}_{\Sigma F}^{j} = \underline{\underline{Y}}_w^{a_{j-1}} \cdot \vec{E}_t^{a_{j-1}} - \left(\vec{J}_{eff}^{a_{j-1}} + \vec{K}_{eff}^{a_{j-1}}\right) \tag{4.14}$$

where $\vec{K}_{eff}^{a_{j-1}}$ takes into account the currents in all conductors closer to the wall. The next step to the layer $x = -a_j$ is similar to the first step, except for the initial conditions. First the fields on the inner side of the j–th conductor, $x = -a_j^-$, are obtained from those at the plane $-a_{j-1}^+$ using Eq. (4.5): proceeding as in section 3.4, but taking into account the contributions from the radial currents, we obtain

$$\begin{aligned} \vec{B}_t^{a_j^-} + \frac{i}{\nu_x}\vec{J}_{SF}^{j} &= \underline{\underline{Y}}_w^{a_j} \cdot \vec{E}_t^{a_j} \\ &- \cosh \nu_x(a_{j-1} - a_j)\left(\underline{\underline{I}} + \nu_x \tilde{T}(a_{j-1} - a_j)\underline{\underline{M}} \cdot \underline{\underline{Y}}_w^{a_j}\right) \cdot \left(\vec{J}_{eff}^{a_{j-1}} + \vec{K}^{a_{j-1}}\right) \end{aligned} \tag{4.15}$$

where

$$\underline{\underline{Y}}_w^{a_j} = \underline{\underline{\Gamma}}_{a_{j-1}}^{a_j} \cdot \left(\underline{\underline{\Lambda}}_{a_{j-1}}^{a_j}\right)^{-1} \tag{4.16}$$

with

$$\begin{aligned} \underline{\underline{\Lambda}}_{a_{j-1}}^{a_j} &= \underline{\underline{I}} - \nu_x \tilde{T}(a_{j-1} - a_j)\underline{\underline{M}} \cdot \underline{\underline{Y}}_w^{a_{j-1}} \\ \underline{\underline{\Gamma}}_{a_{j-1}}^{a_j} &= \underline{\underline{Y}}_w^{a_{j-1}} - \nu_x \tilde{T}(a_{j-1} - a_j)\underline{\underline{N}} \end{aligned} \tag{4.17}$$

Once more, $\underline{\underline{Y}}_w^{a_j}$ is the wave admittance matrix at the plane $x = -a_j$ looking toward the wall, obtained from $\underline{\underline{Y}}_w^{a_{j-1}}$ using the rules for impedance transformations, independently from the presence of source currents.

We can now proceed to the outer side of the j–th conductor by using the jump condition $\vec{B}_t^{a_j^+} = \vec{B}_t^{a_j^-} - \vec{J}_t^{a_j}$. Taking into account the definitions of $\vec{J}_{SF}^{j}$ and $\vec{J}_{eff}^{a_j}$, it is immediate to rearrange the sum over radial currents so that the equation for the fields at the plane $x = -a_j^+$

$$\vec{B}_t^{a_j^+} + \frac{i}{\nu_x}\vec{J}_{\Sigma F}^{j+1} = \underline{\underline{Y}}_w^{a_j} \cdot \vec{E}_t^{a_j} - \left(\vec{J}_{eff}^{a_j} + \vec{K}^{a_j}\right) \tag{4.18}$$

has the same form as (4.14) if $\vec{K}^{a_j}$ is evaluated iteratively as:

$$\vec{K}^{a_j} = \cosh \nu_x (a_{j-1} - a_j) \left\{ \underline{\underline{I}} + \nu_x \tilde{T}(a_{j-1} - a_j) \underline{\underline{Y}}_w^{a_j} \cdot \underline{\underline{M}} \right\} \cdot \left(\vec{J}_{eff}^{a_{j-1}} + \vec{K}^{a_{j-1}} \right) \quad (4.19)$$

with $\vec{K}^{a_1}$ given by Eq. (4.11).

3) The last step gives a relation between the fields on the conductors facing the plasma and the currents in all conductors:

$$\vec{B}_t^{a_N^+} = \underline{\underline{Y}}_w^{a_N} \cdot \vec{E}_t^{a_N} - \left(\vec{J}_{eff}^{a_N} + \vec{K}^{a_N} \right) \quad (4.20)$$

where we have taken into account that there are no feeders outside this layer. On the other hand, at this plane looking towards the plasma we must also have

$$\vec{B}_t^{a_N^+} = \underline{\underline{Y}}_p^{a_N} \cdot \vec{E}_t^{a_N} \quad (4.22)$$

where $\underline{\underline{Y}}_p^{a_N}$ is obtained from $\underline{\underline{Y}}^p$ using (3.22). Combining these two conditions and solving for $\vec{E}_t^{a_N}$ we get:

$$\vec{E}_t^{a_N} = \underline{\underline{\mathcal{R}}}^{a_N} \cdot \left(\vec{J}_{eff}^{a_N} + \vec{K}^{a_N} \right) \quad (4.23)$$

with

$$\underline{\underline{\mathcal{R}}}^{a_N} = \left(\underline{\underline{Y}}_w^{a_N} - \underline{\underline{Y}}_p^{a_N} \right)^{-1} = \underline{\underline{Z}}_p^{a_N} \cdot \left(\underline{\underline{Z}}_p^{a_N} - \underline{\underline{Z}}_w^{a_N} \right)^{-1} \cdot \underline{\underline{Z}}_w^{a_N} \quad (4.24)$$

The second form is well–behaved even if $\underline{\underline{Z}}_p$ is singular (e.g. when $n_z = 0$, or when propagation in the plasma is described in the zero electron inertia approximation); as a consequence it should be preferred for numerical applications.

4) Once $\vec{E}_t^{a_N}$ is known, the fields at any other plane in vacuum can be easily obtained using Eq. (4.5). In particular, the values $\vec{E}_t^p$ and $\vec{B}_t^p$ at $x = 0$ must be used to impose the continuity of the fields at the plasma edge. This condition is simply once more $\vec{E}_t^p = \underline{\underline{Z}}_p \cdot \vec{B}_t^p$, and determines the solution inside the plasma, i.e. which linear combination of the two independent physically acceptable solutions already used to evaluate $\underline{\underline{Z}}_p$ is actually excited by the given external currents. Moreover, if the currents are considered as given instead of being evaluated selfconsistently, substituting $\vec{E}_t^p$, $\vec{B}_t^p$ into Eq. (3.10) directly gives the radiation resistance and the power spectrum.

The variational functional (2.16) or its generalisation (2.28) can easily be constructed using the results of this section. If there is only one layer of conductors in the plane $x = -a$, then $\underline{\underline{\mathcal{R}}}^a(n_y, n_z)$ is explicitly given by Eq. (4.24). Otherwise one must determine the field at each additional sheet of conductors by solving step by step Eqs. (4.5) backwards, taking into account the jump conditions as appropriate:

$$\vec{E}_t^{a_j} = \cosh \nu_x (a_j - a_{j+1}) \left\{ \underline{\underline{\Lambda}}_{a_j}^{a_{j+1}} \cdot \vec{E}_t^{a_{j+1}} + \nu_x \tilde{T}(a_j - a_{j+1}) \underline{\underline{M}} \cdot \vec{K}_{eff}^{a_{j+1}} \right\} \quad (4.25)$$

and add the corresponding contribution $\vec{J}_t^{a_j *} \cdot \vec{E}_t^{a_j}$ to the variational functional. A simple calculation also gives the contribution to (2.16) from feeders and shorts:

$$Z_{Feeds} = \frac{4\pi^2 R_p r_p}{I_A^2} \sum_{n_y} \sum_{n_z} \sum_{j=1}^{N_c} \left\{ \vec{J}_x j * \cdot \left[\frac{1 - \cosh \nu_x (a_{j-1} - a_j)}{\nu_x} \left(\vec{n}_t \cdot \underline{\underline{N}} \cdot \vec{E}_t^{a_j} \right) \right.\right.$$

$$\left.\left. - \frac{\sinh \nu_x (a_{j-1} - a_j)}{\nu_x} \vec{n}_t \cdot \left(\underline{\underline{Y}}_w^{a_j} \cdot \vec{E}_t^{a_j} - \vec{K}_{eff}^{a_j} \right) \right] + \frac{i}{\nu_x^2} (a_{j-1} - a_j) |J_x^{a_j}|^2 \right\} \tag{4.26}$$

where $\vec{n}_t = n_y \vec{u}_y + n_z \vec{u}_z$. Although in the general case the explicit expression for $\underline{\underline{\mathcal{R}}}^a$ is rather complicated, it is clearly quite easy to implement the procedure numerically.

4.3 – Perfectly conducting wall. The equations of the previous paragraph simplify considerably if the wall is ideally conducting. In this case the wave admittance matrix at the plane $x = -a_j$ is given by Eq. (3.13):

$$\underline{\underline{Y}}_w^{a_j} = -\frac{1}{\nu_x \tilde{T}(w - a_j)} \underline{\underline{N}} \tag{4.27}$$

for all j (cfr. the comments at the end of the previous section). Eq. (4.19) reduces to

$$\vec{K}^{a_j} = \frac{\sinh \nu_x (w - a_{j-1})}{\sinh \nu_x (w - a_j)} \left(\vec{J}_{eff}^{a_{j-1}} + \vec{K}^{a_{j-1}} \right) \tag{4.28}$$

with $\vec{K}^{a_1} = 0$. It is remarkable that in this case the contributions from radial currents reduce to the redefinition (4.13) of the effective current in each main conductor, and to the introduction of an 'effective' magnetic field $\vec{B}_t^{eff} = \vec{B}_t + i\vec{J}_F/\nu_x$. Finally, a few lines of algebra give

$$\underline{\underline{R}}^{a_N} = \frac{\nu_x^2 \tilde{T}^2 (w - a_N) \underline{\underline{Z}}_p^{a_N} + \nu_x \tilde{T} (w - a_N) \det \left(\underline{\underline{Z}}_p^{a_N} \right) \underline{\underline{M}}}{\det \left(\underline{\underline{Z}}_p^{a_N} \right) + \nu_x \tilde{T} (w - a_N) \mathrm{Tr}\, \underline{\underline{N}} \cdot \underline{\underline{Z}}_p^{a_N} + \nu_x^2 \tilde{T}^2 (w - a_N)} \tag{4.29}$$

4.4 – Ideal Faraday shield. An ideal Faraday shield is easily included in the evaluation of the excited fields. Let us assume for simplicity that the shield is located at $x = -s$ ($a_N \geq s \geq 0$), external to all active conductors, with blades inclined by an angle β_s with respect to the static magnetic field. Then in the shield plane

$$\vec{E}_t^s = \vec{u}_{\eta_s} E^s \qquad \vec{J}^s = J^s \vec{u}_{\beta_s} \tag{4.30}$$

where

$$\begin{aligned} \vec{u}_{\beta_s} &= -\sin \beta_s \vec{u}_y + \cos \beta_s \vec{u}_z \\ \vec{u}_{\eta_s} &= -(\vec{u}_x \times \vec{u}_{\beta_s}) = \cos \beta_s \vec{u}_y + \sin \beta_s \vec{u}_z \end{aligned} \tag{4.31}$$

are unit vectors along and perpendicular to the shield blades. If for the moment we suppose that the shield currents are known, we can apply once more the previous procedure, and write

$$\left(\underline{\underline{Y}}^s_w - \underline{\underline{Y}}^s_p\right) \cdot \vec{E}^s_t = J^s \vec{u}_{\beta_s} + \vec{K}^s \tag{4.32}$$

where $\vec{K}^s$ can be obtained from $\vec{K}^{a_N}$ using once more Eq. (4.19). In contrast to the situation at active conductors, however, in this equation the unknowns are E^s and J^s, rather than the two components of the tangential wave field. Taking components along $\vec{u}_{\beta_s}$ and $\vec{u}_{\eta_s}$ it is not difficult to obtain

$$J^s = -\frac{\left(\vec{u}_{\beta_s} \cdot \underline{\underline{R}}^s \cdot \vec{K}^s\right)}{\left(\vec{u}_{\beta_s} \cdot \underline{\underline{R}}^s \cdot \vec{u}_{\beta_s}\right)} \tag{4.33}$$

and

$$E^s = \left(\vec{u}_\eta \cdot \underline{\underline{R}}^s \cdot \vec{u}_{\beta_s}\right) J^s + \left(\vec{u}_\eta \cdot \underline{\underline{R}}^s \cdot \vec{K}^s\right) \tag{4.34}$$

with

$$\underline{\underline{R}}^s = \underline{\underline{Z}}^s_p \cdot \left(\underline{\underline{Z}}^s_p - \underline{\underline{Z}}^s_w\right)^{-1} \cdot \underline{\underline{Z}}^s_w \tag{4.35}$$

which is of course the same as (4.24) with $x = -s$ replacing $x = -a_N$. It can moreover easily be written in a form analogous to (4.29) if the back wall is ideally conducting.

According to Eq. (4.34), E^s vanishes if all the source currents are parallel to the direction of the screen blades: in this case the field is confined between the screen and the wall. By contrast, even if all source currents are orthogonal to the direction of the screen blades, J^s does not vanish, unless the partial wave considered is strictly TE or TM in a reference frame with axes oriented along $\vec{u}_\beta$, $\vec{u}_\eta$. Nevertheless, since $\vec{E}^s_t$ and $\vec{J}^s$ are orthogonal to each other, an ideal Faraday screen does not contribute to the variational functional (except indirectly by modifying the fields at the active conductors).

5 – Examples.

5.1 – Implementation of the variational procedure. In the following we will consider two common antenna configurations, sketched in fig. 1, as well as a more complicated configuration which models the antenna to be used for ICR heating in ASDEX Upgrade[28], described below. The first standard antenna is a single conducting strip shorted at the center and feeded in push–pull at both ends. If ℓ_a and w_a are the half–length and the width of the conductor, respectively, the transmission–line model suggests a current distribution of the form

$$J_\eta(\eta) = \frac{I_A}{w_a} \frac{\cos(k_o \nu_a \eta)}{\cos(k_o \nu_a \ell_a)} \tag{5.1}$$

(auxiliary coordinates η along the main conductor, ζ across it, are used in the antenna plane). Oriented poloidally ($\eta \equiv y$), this is the typical element of fast wave IC launchers. An antenna of this kind has been used in ASDEX[30]. The second standard configuration is a T–antenna feeded at the center and shorted at the ends, with an antisymmetric current distribution for which the transmission–line model gives

$$J_\eta(\eta) = \frac{I_A}{2w_a} \operatorname{sign}(\eta) \frac{\cos k_o \nu_a (|\eta| - \ell_a)}{\cos k_o \nu_a \ell_a} \tag{5.2}$$

Oriented toroidally ($\eta \equiv z$), this is the typical launcher for Ion Bernstein waves.

To write Eqs. (5.1) and (5.2), one regards the antennas as a segment of transmission line characterised by the distributed inductance L, capacitance C and resistance R per unit length. In this approximation, The propagation constant ν_a is then given by

$$k_o \nu_a = \sqrt{i\omega C(-i\omega L + R)} \simeq \omega\sqrt{LC}\left(1 + \frac{i}{2}\frac{R}{\omega L}\right) \tag{5.3}$$

In addition, the boundary condition $dJ_\eta/d\eta = 0$ must be imposed at shorts.

The variational method is most simply implemented by making Z_a stationary with respect to ν_a in Eqs. (5.1) and (5.2). This procedure has the advantage that the propagation constant is in principle accessible to measurement. It should be noted however that the assumption that ν_a is real is justified only if $R \ll \omega L$; this approximation is also essential to avoid the cumbersome determination of the hermitean adjoint operator $\mathcal{R}^{a\dagger}$.

The Ritz method is similarly implemented using sinusoidal functions satisfying the boundary conditions at shorts, but with arbitrarily chosen basic periodicity, and allowing for a few harmonics. Since the superposition has complex coefficients, one generally finds in the main conductor a small current in quadrature with the feeder current.

Nevertheless for a single element antenna the two approaches not only give very similar values for R_a and Z_a, but also predict very similar current distributions. When this is the case, an 'effective' propagation constant ν_a can be estimated also within the Ritz method, by fitting the ratio of feeder to peak current with that predicted by a transmission line approximation of the form (5.1) or (5.2). In other cases however, for example for 'dipole' antennas, a direct variation gives rather poor results, and the Ritz approach is definitely superior.

Before proceeding to the examples, let us make a few comments on the accuracy and efficiency of the numerical codes. The direct variational procedure is implemented by 'brute force', i.e. by evaluating Z_a for all values of ν_a in an appropriate interval and looking for the stationary point. With a good vectorialisation of the ν_a loop, a complete case requires 10 to 20 seconds. The Ritz approach is appreciably faster, being essentially equivalent to a run of the direct variation method using only a few values of ν_a. By far the heaviest task is the evaluation of the surface impedance matrices of the plasma. In the fast–wave cases for example we have taken 81 toroidal and 21 poloidal Fourier components; integrating the wave equations for each partial wave across the whole Asdex Upgrade cross-section (105 cm including the scrape–off plasma) takes about 3 minutes on a CRAY YMP. An advantage of the present formulation is that this has to be done only once for given plasma parameters; the results can then be used for any antenna.

There are several accuracy checks available in the code. The comparison of the power radiated by the antenna (the numerator of Eq. (1.1)) with the power found in the plasma gives an estimate of the accuracy of the integration of the wave equations. Typically, we chose the mesh step so that this error, summed over the whole spectrum, is of the order of 10^{-5}. The error made by truncating the sums over poloidal and toroidal modes is more difficult to estimate: the resistive part of Z_a converges very rapidly, but the reactive part converges somewhat slowly. From the tests made, we hope to have reached convergence to within a few percent in all cases. The accuracy of the solution of the matching equations in vacuum is typically of 7 significant digits or better; it deteriorates somewhat at very low frequencies ($\lesssim 1$ Mhz).

Finally, a word should be said about the convergence of the Ritz expansion. As in reference[20], we find that the Ritz method gives results fairly independent from the basic periodicity chosen for the test functions. It also converges rapidly, in the sense that for example the current distributions obtained using 3 or 4 modes typically agree within one or two percent; the values of Z_a are much closer. The number of harmonics taken into account however should not be increased beyond what is compatible with the

truncation of the series in the Fourier decomposition of the radiated field. If the Fourier transform of the antenna current (2.13) contains wavevectors larger than those actually included in the representation of the radiated field in the plasma, the system (2.17) becomes ill–conditioned, and the results can no more be trusted. It is useful to regard the Ritz representation (2.13) of the antenna current as an improvement over the simple transmission line representation (5.1) or (5.2), which takes into account reflection and excitation of higher modes of the transmission line at discontinuities (feeders and shorts). It is this additional freedom in the choice of test functions which makes the force of the Ritz approach; however this advantage can only be used if information is available on how these modes are radiated.

For convenience, a fast version of the code which deals only with antennas radiating in the absence of plasma has also been written. It is assumed that a metallic wall faces the antenna at a distance $x = 2r_p$: the antenna is then in a box with toroidal topology, although curvatures are neglected. To have a meaningful problem, it is necessary in this case to take into account the resistivity of the walls. The impedance and admittance matrices of a resistive wall are given by Eqs. (3.14).

5.2 – Single element antennas radiating in vacuum. Teilhaber and Jacquinot[20] have shown that at low frequency the variational procedure reproduces the results of the transmission–line model in the the quasi–static limit for a simple antenna radiating in vacuum, bare or with Faraday Shield. Since in vacuum our formulation is completely equivalent to theirs, we omit the details. We note however that this statement holds only in the limit in which the Fourier spectre of the radiated field is continuous. If the antenna radiates into a toroidal vessel of finite dimensions, the transmission–line model breaks down for frequencies close to eigenfrequencies of the vacuum cavity. This is illustrated in figs. 2 and 3. Fig. 2 shows ν_a, R and $Z = \mathrm{Im}\,(Z_a)$ versus frequency for the antenna of the ASDEX ICRF experiment[30] (half-length $\ell_a = 49.5$ cm, width $w_a = 18$ cm, distance from the wall $a = 7.6$ cm, distance from the Faraday shield $s - a = 1.6$ cm), radiating in the ASDEX vessel (diameter 0.95 m, major radius 1.65 m). The results for a T–antenna of the same dimensions are shown in Fig. 3. The agreement between the direct variation of ν_a (open squares) and the Ritz method (full squares) is excellent at low frequencies, and deteriorates slightly at higher frequencies. The loading resistance is due mainly to dissipation in the back wall, which is in the near region for a broad spectrum of evanescent waves (dissipation in the antenna itself is not included). The behaviour of R_a around $f = 28$ and $f = 56$ Mhz is characteristic of the excitation of high quality cavity eigenmodes: those seen in the figures can be identified as having toroidal wavenumber $n_\varphi = 1$ and 2, respectively. The main contribution to the resonances comes from modes

with $n_\parallel^2$ close to unity, which are well guided along the wall and the Faraday screen; the importance of these modes is likely to be overestimated because of the idealised geometry. In the limit of a continuous spectrum these modes can be discarded by treating the associated singularities as principal parts[6]. Unfortunately, this procedure cannot be easily generalised to the case of a discrete spectre: this is in our opinion one of the weakest points of the plane layered approximation. Note that in the vicinity of the resonant frequencies the direct method fails, while the Ritz approach remains valid, although it is not possible to define ν_a for the resulting current distributions.

5.3 – Dipole antenna radiating in vacuum. Antennas with two identical parallel conductors allow some spectral shaping, a desirable feature in several ICRH scenarios. Most commonly, the two conductors are excited with opposite phases, so as to launch an antisymmetric n_z spectrum and suppress modes with $n_z^2 \simeq 0$: this configuration is known as a 'dipole' antenna.

Fig. 4 shows R and Z versus frequency for a dipole antenna of the ASDEX type in the resistive box, with a gap $w_g = 16$ cm between the two conductors (such an antenna was not used in the experiments). The behaviour is similar to that of the single conductor antenna, except that cavity eigenmodes are less excited, since low n_φ components are much less represented in the antisymmetric current spectrum.

For a dipole antenna with two push–pull elements, a direct variation of ν_a (which for symmetry must be the same in both conductors) often fails: the only stationary point is found to be $\nu_a = 0$, corresponding to a constant current along each conductors. The current distribution obtained with the Ritz method has an appreciably larger content in higher harmonics than in the 'monopole' case, so that the current in the feeders can be slightly larger than the current at the central short. When this is the case, the best approximation with the ansatz (5.1) occurs indeed for $\nu_a = 0$; it is however clear that this class of test functions is too restrictive.

5.4 – Plasma loaded fast–wave antenna. A frequency scan for a plasma–loaded antenna is hardly meaningful, since for a given magnetic field and plasma composition the cyclotron resonance conditions are satisfied only in discrete frequency intervals. Instead, we have chosen a typical minority heating scenario (H^+ in D^+, $f = 45$ Mhz, $B_o = 3$ T), and varied the minority concentration and the antenna configuration. The plasma parameters were taken to be: central density $8\,10^{19}$ m^{-3}, central temperature 2 keV for D^+ and electrons, 3.6 keV for H^+. The plasma model consists of the Colestock–Kashuba Finite Larmor radius equations[31], enlarged to take into account electron Landau and Transit Time damping[26], as well as collisional damping.

Figs. 5 (R and Z) and 6 (power repartition between species) compare the standard ASDEX ICRH antenna in the monopole and dipole configurations; the power spectra, $P(n_\varphi)$, are shown in figs. 7 for the two cases. In a pure D^+ plasma the single transit absorption is rather weak, and several global eigenmodes are excited. At moderate H^+ concentration low n_ϕ modes are converted into Bernstein waves, while higher n_ϕ modes are efficiently absorbed by the minority, so that the single transit absorption is large, although not complete; as a consequence the radiated spectra do not show strong eigenmodes, and are similar, although not identical, to those which would be obtained by imposing outward radiation conditions before the resonance layer (equivalent to the assumption of complete single pass absorption). The single pass absorption deteriorates rapidly again as $n_H/n_e \gtrsim 0.10$, since the evanescence layer associated to the ion–ion resonance becomes optically thick. In this regime strong eigenmodes are excited between the outer wall and the ion–ion cut–off, while the h.f. field at the cyclotron resonance is very low: as a consequence electron heating (transit time and collisional) dominates again over minority heating. The eigenmodes also clearly affect the antenna resistance. The largest contribution to the loading is always due to eigenmodes with low n_φ, wich are also less subject to damping by the ions; therefore both the peak in R and in electron absorption are more pronounced in the monopole than in the dipole configuration.

Note that under these conditions it is very difficult to influence the shape of the spectrum with two conductors only: the n_ϕ–selectivity associated with the excitation of eigenmodes completely masks the differences due to the antenna configuration. It should nevertheless be mentioned that the role of eigenmodes is likely to be overestimated in the plane–stratified geometry in which these calculations are made. Eigenmodes have ben observed in ASDEX[32], but are associated with a rather modest increase of loading resistance. By contrast, other predictions of the FELICE code are well confirmed experimentally, in particular an appreciable increase of direct electron heating in the outer part of the plasma under conditions of low single pass absorption[33]. The tendency of the plane layered model to overestimate eigenmodes is due in part to the fact that absorption of low n_φ components is underestimated: in toroidal geometry even the mode $n_\varphi = 0$ is seen by the plasma as having a rather broad $k_\parallel$–spectre, and therefore suffers appreciable cyclotron damping[34].

In spite of the large variation in the loading resistance and in the launched spectra, the reactive part of the antenna impedance Z remains nearly constant throughout the concentration scan, and close to the value without plasma. Experimentally Z was not measured, but is known to change little with loading conditions. This corresponds also to the expectation that at low frequencies the distributed capacitance and inductance

of the antenna should be determined essentially by the geometry of wall, conductors, and Faraday shield only.

5.5 – The ASDEX Upgrade ICRH antenna. The formalism of the previous sections is particularly useful to evaluate antennas with two or more 'layers' of conductors, such as the one which will be used for ICRH in ASDEX Upgrade (fig. 8). A dipole–like configuration (toroidally antisymmetric, but not identical with the one considered above) will be obtained using two such elements oppositely oriented and excited in phase. The plane layered model of one element is sketched in fig. 9. The current distribution corresponding to the transmission line model is easily written using a coordinate ξ along the conductors with origin at the shorts, as indicated in the figure. If I_u and I_d denote the current in the upper and lower loop, respectively, and w_a the width of the conductors, we have:

1) UPPER LOOP. We count the distance ξ along this loop from the middle–plane short placed at $y = 0$. Then in the main conductor $\xi = y$, and in the return conductor $\xi = 2L_u - y$ ($y_F \leq y \leq L_u$; the length of the radial section must be omitted since the radial current was assumed to be constant in paragraph 4.1). Hence:

Feeder:

$$J_x = \frac{I_u}{w_a}\,\delta\,(y - y_F) \qquad 0 < x < x_1 \tag{5.4}$$

Return conductor, above the feeder:

$$J_y = \frac{I_u}{w_a}\,\frac{\cos\kappa_u(2L_u - y)}{\cos\kappa_u(2L_u - y_F)} \qquad y_F < y < L_u \tag{5.5}$$

Upper radial section:

$$J_x = \frac{I_u}{w_a}\,\frac{\cos\kappa_u L_u}{\cos\kappa_u(2L_u - y_F)}\,\delta\,(y - L_u) \qquad x_2 < x < x_1 \tag{5.6}$$

Main conductor, upper half:

$$J_y = -\frac{I_u}{w_a}\,\frac{\cos\kappa_u y}{\cos\kappa_u(2L_u - y_F)} \qquad 0 < y < L_u \tag{5.7}$$

Middle radial section:

$$J_x = -\frac{I_u}{w_a}\,\frac{1}{\cos\kappa_u(2L_u - y_F)}\,\delta\,(y) \qquad 0 < x < x_2 \tag{5.8}$$

2) LOWER LOOP. We count the distance ξ along the antenna from the lower short. The inner–outer connection is at $y = -\delta$. Then in the main conductor $\xi = L_d + y$ with $-L_d \leq y \leq -\delta$, and in the return conductor $\xi = L_d + y$) with $(-\delta \leq y \leq y_F$. Hence:

Feeder:

$$J_x = \frac{I_d}{w_a}\,\delta\,(y - y_F) \qquad 0 < x < x_1 \tag{5.9}$$

Return conductor, below the feeder:

$$J_y = -\frac{I_d}{w_a}\,\frac{\cos\kappa_d(L_d + y)}{\cos\kappa_d(L_d + y_F)} \qquad -\delta < y < y_F \tag{5.10}$$

Middle radial section, contribution from the lower loop:

$$J_x = \frac{I_d}{w_a}\,\frac{\cos\kappa_d(L_d - \delta)}{\cos\kappa_d(L_d + y_F)}\,\delta\,(y - \delta) \qquad x_1 < x < x_2 \tag{5.11}$$

Main conductor, lower half:

$$J_y = -\frac{I_d}{w_a}\,\frac{\cos\kappa_d(L_d + y)}{\cos\kappa_d(L_d + y_F)} \qquad -L_d < y < -\delta \tag{5.12}$$

Lower radial section:

$$J_x = -\frac{I_d}{w_a}\,\frac{1}{\cos\kappa_d(L_d + y_F)}\,\delta\,(y + L_d) \qquad 0 < x < x_2 \tag{5.13}$$

In the examples, we have supposed for simplicity that the two loops are balanced, so that $I_u = I_d$. To investigate possible lack of balance the results of section 2.4 should be used; this extended formalism however is not implemented in the code.

Frequency scans without plasma for a single conductor and for the dipole configuration of this type are shown in fig. 10. Above $\simeq 80$ Mhz the impedance of the single conductor changes from inductive to capacitive, a behaviour in agreement with a detailed Finite Element analysis[29]. The ASDEX Upgrade antenna becomes resonant at $f \simeq 100$ Mhz: this gives the upper usable frequency, since for proper matching it is important that the current seen by the plasma should not change sign. As shown in fig. 11 this condition is still well satisfied at 80 Mhz, although appreciable deviations from a uniform distribution can already be seen, particularly in the dipole configuration.

The characteristics of the ASDEX Upgrade antenna with plasma loading at 45 Mhz are shown in fig. 5 (triangles). The loading resistance is similar to that of the conventional ASDEX antenna, with slightly higher values in the dipole case (we recall however that this is by definition the radiation resistance of the whole antenna, with the four 'arms' in parallel. In the experiment the resistance measured is that of each element separately, which is just 4 times larger, disregarding slight asymmetries between elements). The power spectra and the distribution of heating among species are also very similar to those shown in figs. 6 and 7.

5.6 – Bernstein wave launching. The self–consistent determination of the antenna current appears to be particularly important in the case of ion Bernstein wave launching. In this case the main antenna conductors must be oriented along the toroidal direction[12], so that the details of the antenna current distribution influence directly the n_z spectrum. Since the surface admittance of the plasma for IB waves is a sensitive function of n_z [12], this in turn can have a much larger effect on the loading resistance than in the case of fast wave launching.

To investigate this case we have considered a Deuterium plasma with the same parameters as before, and a T antenna with the same dimensions as in section 5.2, but oriented toroidally. Although the theory of IB waves launching has recently been extended to higher harmonics[35]–[36], we have limited ourselves here to the case $\omega \simeq 2\Omega_c$, for which the Finite Larmor Radius code FELICE can be used without modification. The second cyclotron harmonic of D^+ crosses the plasma edge when the applied frequency is 34.3 Mhz; one expects excitation of the first IB wave at frequencies slightly lower than this value, when the IC resonance is situated just behind the antenna. This is confirmed by fig. 12 b, which shows that in the range 33.6 Mhz $\lesssim f \lesssim$ 34 Mhz between 50 and 80 % of the power is radiated in the Bernstein branch. At higher frequencies some harmonic IC damping occurs in the scrape–off plasma, while at too low frequencies the wavelength of the IB wave at the plasma boundary becomes too short for good matching. The range in which IB waves can be directly excited is therefore unconfortably narrow.

More surprising is the fact that no appreciable variation of the loading resistance is found over the whole frequency range (fig. 12 a). If the Faraday screen is in direct contact with the plasma, R is consistently less than 0.1 Ohm. On the other hand both R and the reactive impedance Z (which is low and capacitive) are sensitive functions of the distance of the Faraday screen from the plasma edge (fig. 13). Thus if ponderomotive forces or protective limiters were to create a vacuum layer of a few millimeter before the antenna, the loading would increase to about 0.5 Ohm; it would further increase to more than 1.5 Ohm if the antenna where rectracted a few cm away from the plasma edge. This behaviour strongly suggests that the loading resistance is dominated by coupling to the fast wave even in the range in which IB waves are excited. The antenna is very badly adapted to launch the fast wave, particularly if the Faraday screen touches the plasma, since this imposes the boundary condition $E_y = 0$ at the plasma surface; a vacuum layer between the Faraday screen and the plasma improves the situation by relaxing this condition. These results confirm the general difficulty of finding situations in which IB waves could be launched efficiently according to theory[12],[35],[36]. We may add that the n_z spectrum of the T antenna considered here, peaking at $n_z \simeq 5$ and

extending to $n_z \lesssim 12$, is about optimised for IB waves launching, and that a reasonably low density, 1.5 10^{11} cm^{-3}, was assumed at the plasma edge.

As already mentioned, the results of fig. 13 show that the characteristics IB wave antennas are appreciably affected by the distance d_{FP} between antenna and plasma edge. In addition, the effective phase velocity along the conductors is found to be more than 2.5 times slower than the speed of light, so that the current distribution along the antenna, shown for a few typical cases in fig. 14, differs considerably from the one found in the same antenna radiating towards vacuum. In particular, when d_{FP} is sufficiently large, the contribution of the main conductors to the reactive part of the impedance becomes inductive, although not large enough to compensate for the capacitive contribution of feeders and shorts. As a consequence, in this situation $|Z|$ is only about two times R, resulting in an unusually large component of J_η in quadrature with the feeder current. Another consequence of the sensitivity of J_η to the configuration is that in this case the loading resistance corresponding to the self–consistent current distribution is about a factor two larger than the resistance which is found assuming a constant current (by contrast, in the case of fast wave antennas, the error made with this simple Ansatz is typically 10 to 20 %).

Aknowledgments. We thank Dr. J.–M. Noterdaeme fo careful reading of the manuscript and useful suggestions.

References

[1] J. Adam, Report EUR-CEA-FC 1004, 1979.

[2] J. Adam, J. Jacquinot, Y. Lapierre, S. Marty, Proc. 4th top. Conf. on RF Plasma Heating, Austin 1981, , paper A1.

[3] R.R. Weynants, A.M. Messiaen, C. Leblud, P.E. Vandenplas, Proc. 2d Int. Symp. om Heating in Toroidal Plasmas, Como 1980, EUR-7424-EN, Vol. 1, p. 487.

[4] A.M. Messiaen, R. Koch, V.P. Bhatnagar, M. Evrard, P.E. Luwel, E.P. Vandenplas, R.R. Weynants, Proc. 3d Grenoble–Varenna Int. Symp. on Heating in Toroidal Plasmas, Grenoble 1982, EUR-7979-EN Vol. 1, p. 243.

[5] V.P. Bhatnagar, R. Koch, A.M. Messiaen, R.R. Weynants, Nucl. Fus. **22** (1982) 279.

[6] R.R. Weynants Proc 4th Int. Symp. on Heating in Toroidal Plasmas, Roma 1984, Vol. 1, p. 211.

[7] A. Bers, L.P. Harten, A. Ram, Proc. 4th top. Conf. on RF Plasma Heating, Austin 1981, paper A16.

[8] A. Ram, A. Bers, Proc. 3d Grenoble–Varenna Int. Symp. on Heating in Toroidal Plasmas, Grenoble 1982, EUR-7979-EN 1982, vol 1. p. 395.

[9] A. Ram, A. Bers, Nucl. Fus. **24** (1984) 679.

[10] V.L. Vdovin Nucl. Fus. **23** (1983) 1435.

[11] W.N-C. Sy, T. Amano, R. Ando, A. Fukuyama, T. Warai, Nucl. Fus. **22** (1982) 1359.

[12] M. Brambilla, Nucl. Fus. **28** (1988) 549.

[13] M.J. Mayberry, S.C. Chiu, R.I. Pinsker, R. Prater et al., Nucl. Fus. **30** (1990) 579.

[14] V.P. Bhatnagar, D.W. Faulkoner, R. Koch, D.I.C Pearson, Proc. 3d Grenoble–Varenna Int. Symp. on Heating in Toroidal Plasmas, Grenoble 1982, EUR-7979-EN Vol. 1 p. 325.

[15] D.W. Faulconer, J. Appl. Phys **54** (1983) 3810.

[16] F.W. Perkins, Proc 4th Int. Symp. on Heating in Toroidal Plasmas, Roma 1984, Vol 2., p. 1148.

[17] D.N. Smithe, R.J. Kashuba, T. Kammash, J. Appl. Phys **59** (1986) 3980.

[18] I.S. Lehrman, P.L. Colestock, IEEE Trans. Plasma Sci. **PS–15** (1987) 285.

[19] G. Cattanei, A.B. Murphy; Nucl. Fus. **29** (1989) 15.

[20] K. Teilhaber, J. Jacquinot, Nucl. Fus. **24** (1984) 541.

[21] K. Teilhaber, Nucl. Fus. **24** (1984) 1383.

[22] S. Puri, Phys. Fluids **27** (1984) 2156.

[23] S. Puri, Nucl. Fus. **27** (1987) 229.

[24] R.W.P. King, The Theory of Linear Antennas, Harward Univ. Press, Cambridge MA 1956, p. 237.

[25] M. Bures, V. Bhatnagar, S. Corti, G. Devillers et al., Proc. 15th. Europ. Conf. on Contr. Fusion and Plasma Phys., Dubrovnik 1988, Vol. 2, p. 713.

[26] M. Brambilla, Plasma Phys. Contr. Fus. **31** (1989) 723.

[27] T.H. Stix, *The theory of plasma waves,* McGraw–Hill (N.Y.) 1962.

[28] J.-M. Noterdaeme et al., to be published in Fusion Engineering and Design.

[29] M. Söll, F.J. Fischer, J.-M. Noterdaeme, H. Wedler, Finite element calculations for antennas and coaxial lines used in plasma experiments, Proc. 18th MSC Conf. (Prien June 1991), MacNeal and Schwendler, München, 1991.

[30] J.-M. Noterdaeme, M. Söll, F. Wesner et al., Fusion Technology (14th Symp., Avignon) Pergamon Press, Oxford 1986, Vol. 1 p. 795.

[31] P.L. Colestock, R.J. Kashuba, Nucl. Fus. **23** (1983) 763.

[32] Y. Ogawa, F. Hofmeister, J.-M. Noterdaeme et al., Plasma Phys. Contr. Fus. **33** (1991) 155.

[33] F. Ryter, U. Stroth, M. Brambilla et al., Proc. 18th. Europ. Conf. on Contr. Fusion and Plasma Phys., Berlin 1991, Vol. 3 p. 413.

[34] M. Brambilla, T. Krücken, Nucl. Fus. **28** (1988) 1813.

[35] M. Brambilla, A. Cardinali, R. Cesario, Proc. 18th. Europ. Conf. on Contr. Fusion and Plasma Phys., Berlin 1991, Vol. 1 p. 245.

[36] M. Brambilla, A. Cardinali, Nucl. Fus. **32** (1992) to be published.

FIGURE CAPTIONS.

Fig. 1 – Common IC antenna configurations: a) fast wave antenna feeded at both end in push–pull and shorted in the center; b) Bernstein wave antenna with central feeder and shorts at the ends.

Fig. 2 – Frequency behaviour of the ASDEX ICRH antenna (fig. *1 a*) with $\ell_a = 49.5$ cm, $w_a = 18$ cm, without plasma; a) radiation resistance R and impedance Z; b) effective propagation constant ν_a.

Fig. 3 – Frequency behaviour of a T–antenna (fig. *1 a*) of the same dimensions as in fig. 2, shorted at the ends, without plasma: a) radiation resistance R and impedance Z; b) effective propagation constant ν_a.

Fig. 4 – Frequency behaviour of a dipole antenna (two parallel conductors as in Fig. 2, separated by 16 cm and excited in opposition) in a resistive toroidal box. Open squares: resistance R; dotted squares: impedance Z; Ritz method.

Fig. 5 – Impedance Z and resistance R versus minority concentration (Hydrogen in Deuterium; $f = 45$ Mhz, $B_o = 3$ T, $n_e(0) = 8.010^{19}$ m^{-3}, $T_e(0) = T_D(0) = 2$ keV, $T_H = 3.6$ keV). Squares: Asdex antenna; triangles: Asdex Upgrade antenna. Open symbols: monopole; full symbols: dipole configurations.

Fig. 6 – Power absorbed by each particle species versus minority concentration; same plasma as in fig. 6). The power absorbed via mode conversion to Bernstein waves is likely to heat the electrons. a) monopole, b) dipole antenna configuration.

Fig. 7 – Power spectra (normalised to unit total power) from the ASDEX ICRH antenna for different minority concentrations; same plasma as in fig. 6. a) single conductor; b) dipole configuration.

Fig. 8 – The ASDEX Upgrade ICRH antenna.

Fig. 9 – Plane–layered model of the ASDEX Upgrade ICRH antenna.

Fig. 10 – Frequency scan of the ASDEX Upgrade ICRH antenna without plasma. Open squares: R (right scale); dotted squares: Z (left scale).

Fig. 11 – Current distribution in the outer conductors of the Asdex Upgrade antenna at 40 and 80 Mhz. Ritz method, 3 modes.

Fig. 12 – Bernstein wave coupling (pure D^+ plasma as in Fig. 5, edge density 1.5 10^{11} cm^{-3} with e–folding length 1 cm; T–antenna with the same dimensions as in Fig.3, oriented toroidally. a) Loading resistance b) Fraction of power launched in the IB branch and absorbed by harmonic IC dampingversus frequency.

Fig. 13 – Radiation resistance and reactive impedance versus the distance d_{FP} between the Faraday screen and the plasma, for the antenna of fig. 12.

Fig. 14 – Selfconsistent current distribution in the T–antenna of fig. 12.

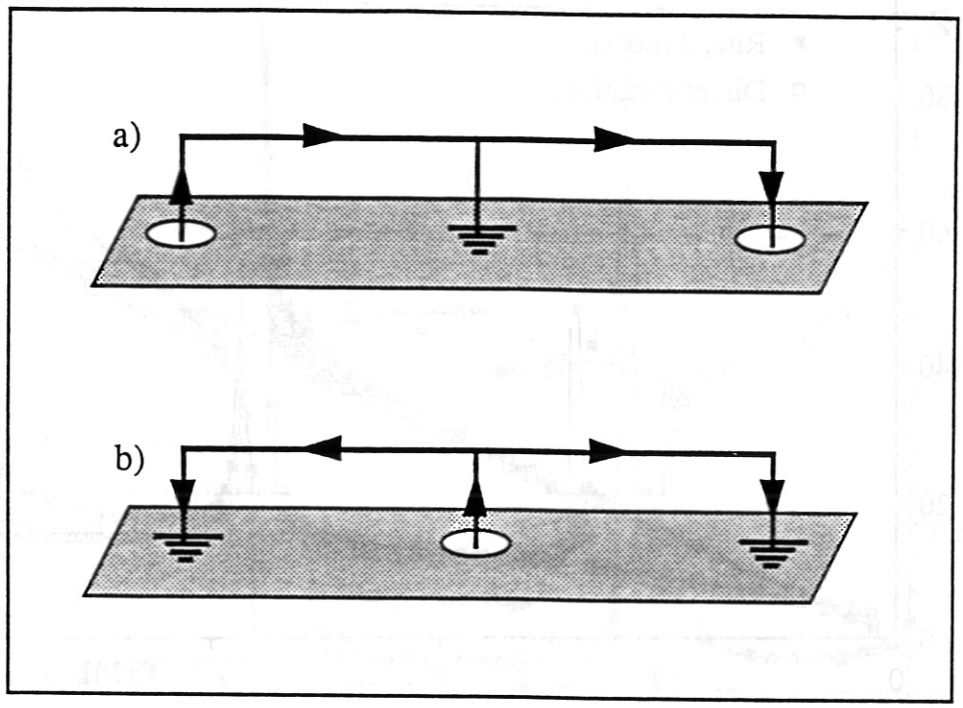

(Fig. 1)

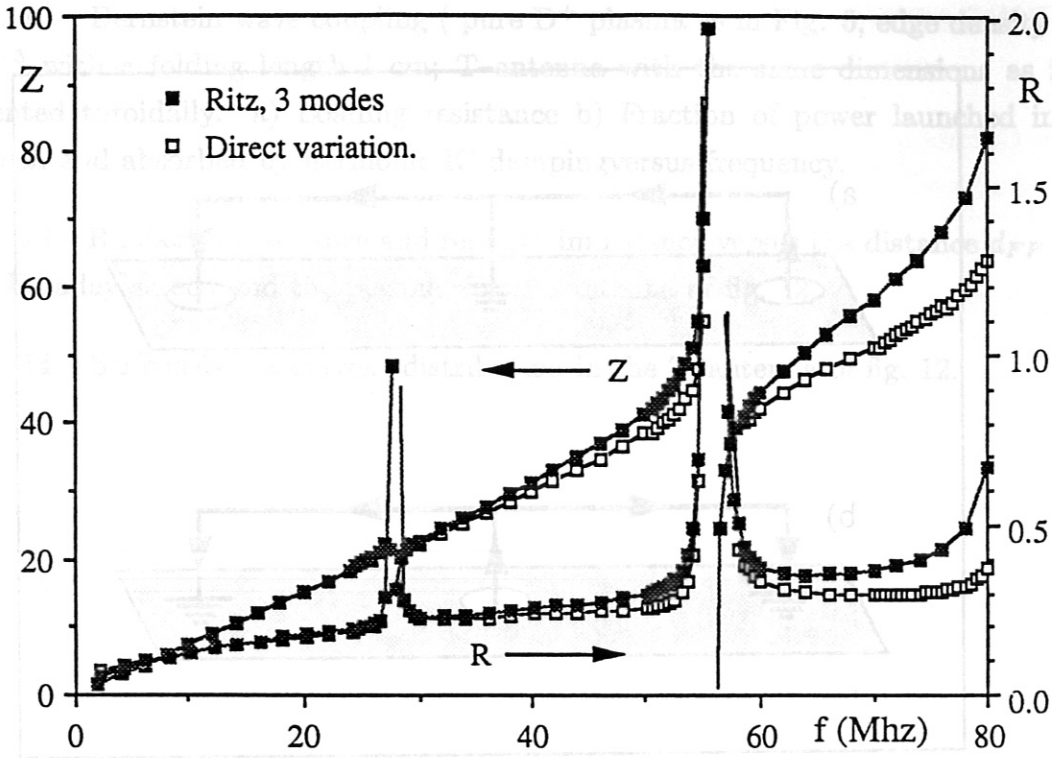
Z
R
Ritz, 3 modes
Direct variation.
Z
R
f (Mhz)
100
80
60
40
20
0
2.0
1.5
1.0
0.5
0.0
0
20
40
60
80

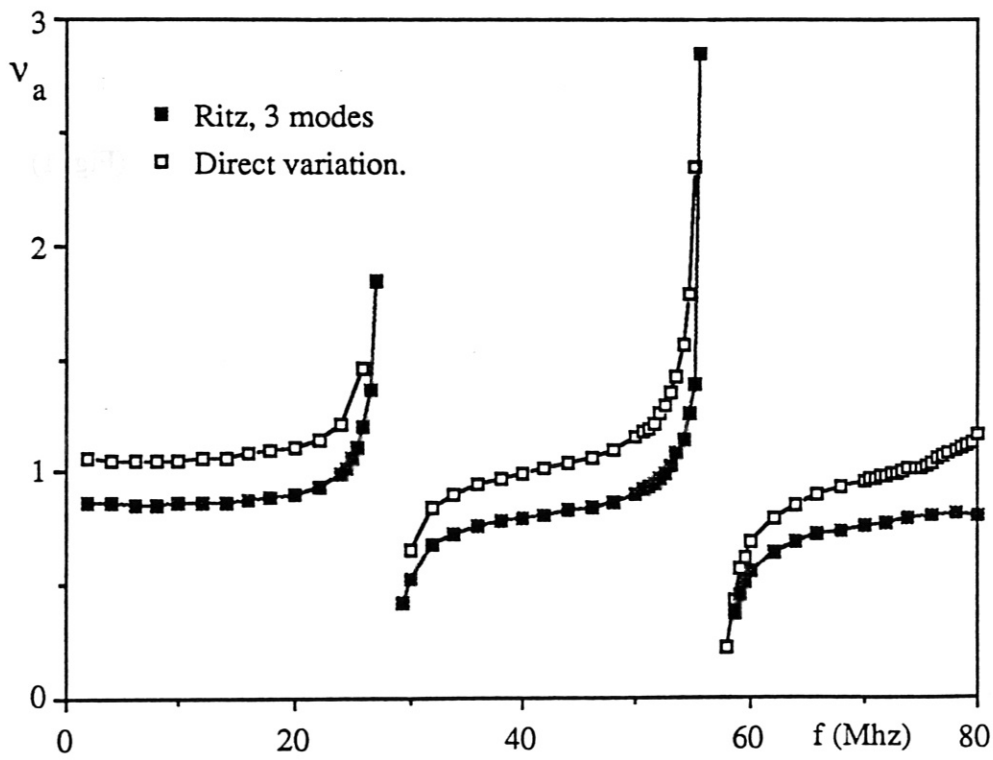
ν_a
Ritz, 3 modes
Direct variation.
f (Mhz)
3
2
1
0
0
20
40
60
80

(Fig.2)

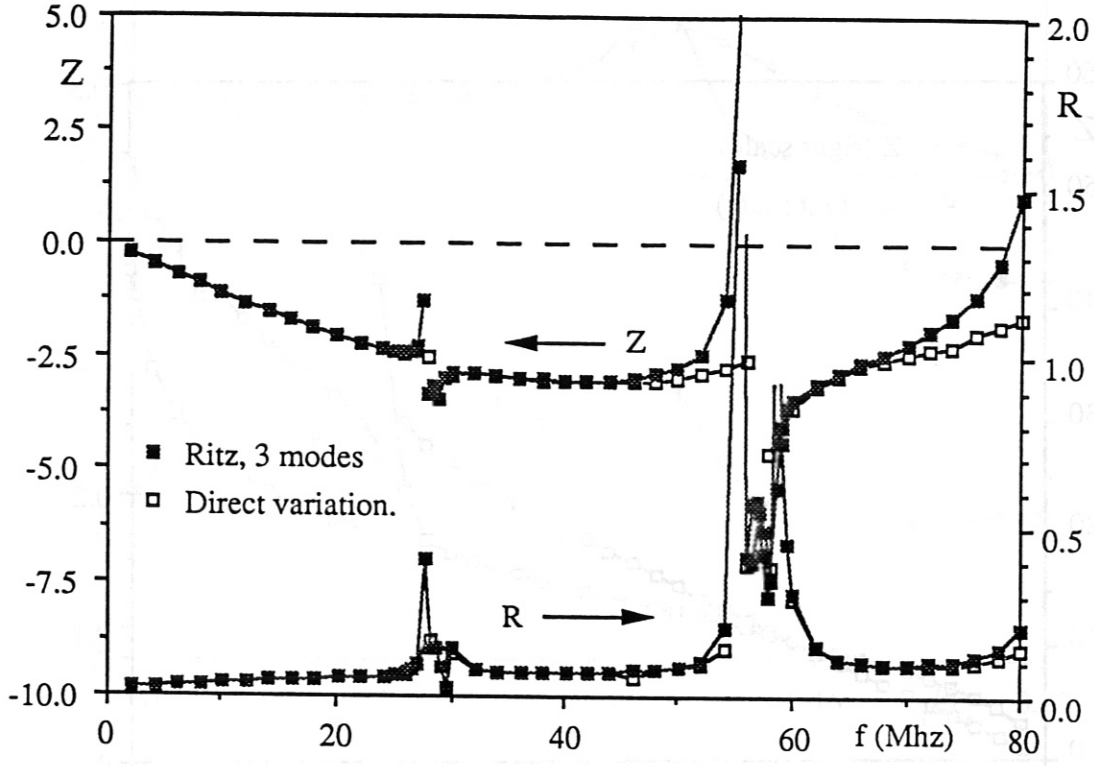
5.0
Z
2.5
0.0
-2.5
-5.0
-7.5
-10.0
2.0
R
1.5
1.0
0.5
0.0
Z
R
Ritz, 3 modes
Direct variation.
0
20
40
60
f (Mhz)
80

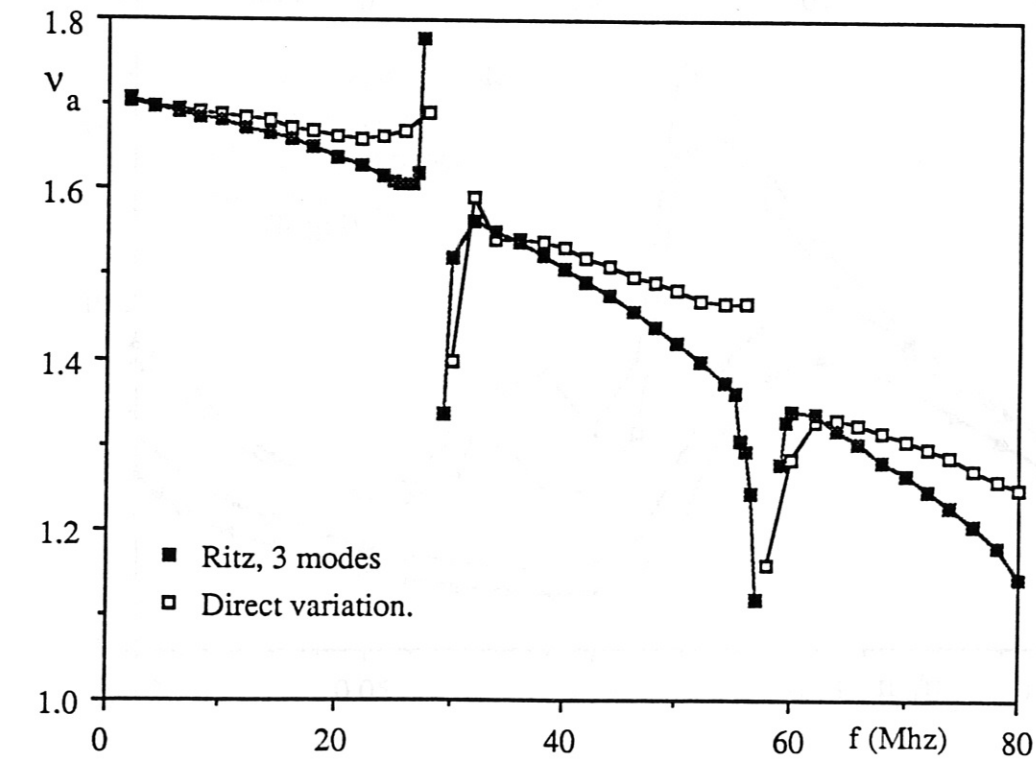
1.8
ν_a
1.6
1.4
1.2
1.0
Ritz, 3 modes
Direct variation.
0
20
40
60
f (Mhz)
80

(Fig. 3)

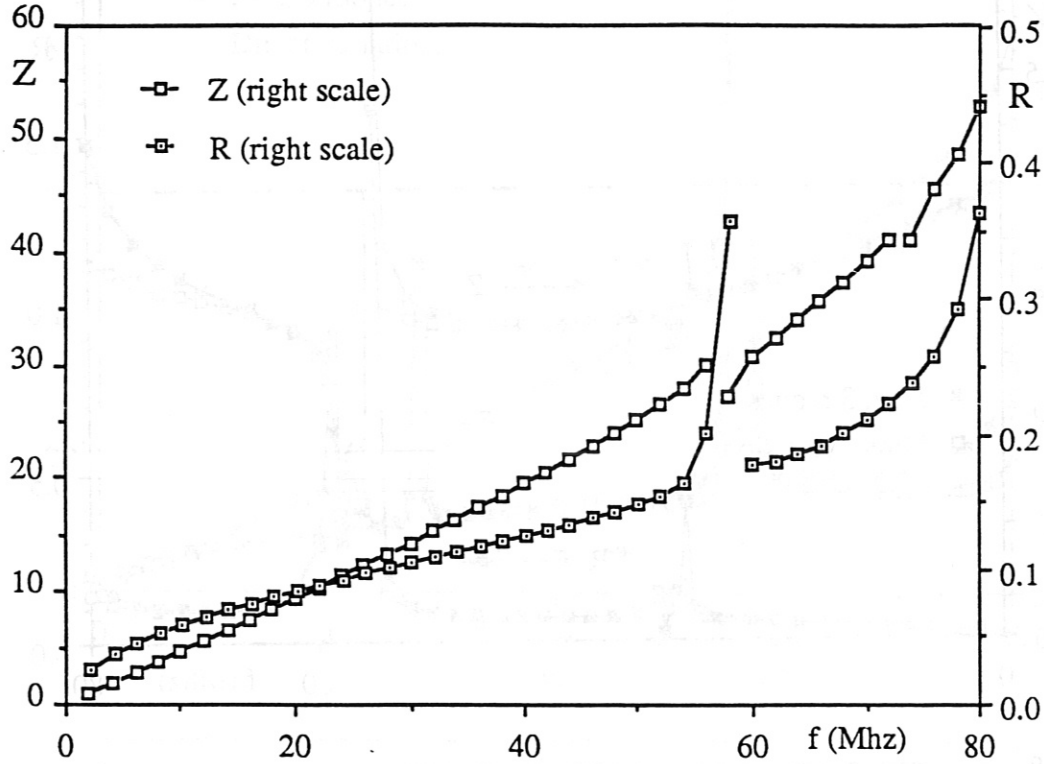
Z
R
Z (right scale)
R (right scale)
60
50
40
30
20
10
0
0.5
0.4
0.3
0.2
0.1
0.0
0
20
40
60
80
f (Mhz)

(Fig. 4)

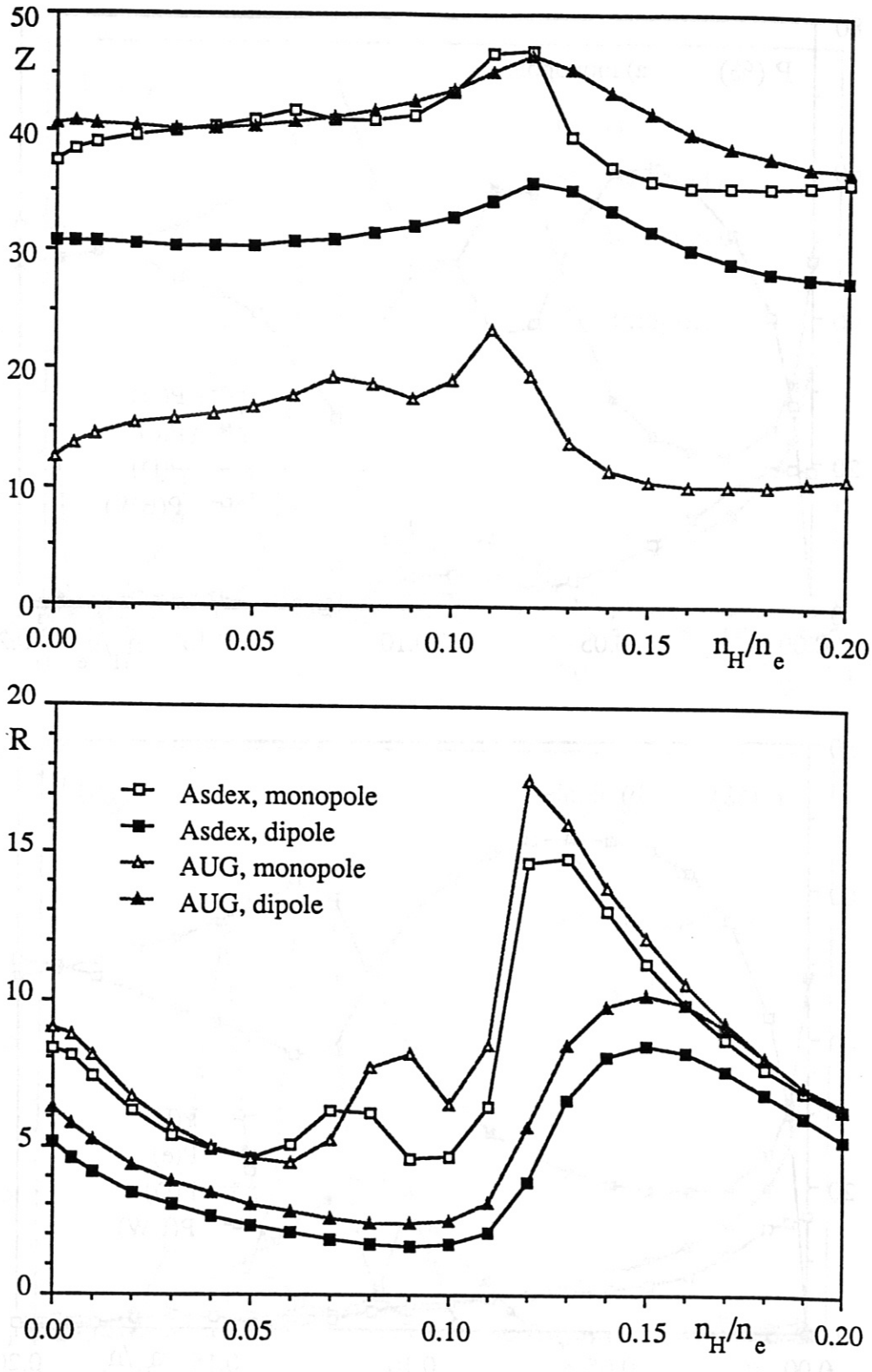
50
Z
40
30
20
10
0
0.00
0.05
0.10
0.15
n_H/n_e
0.20
20
R
15
10
5
0
Asdex, monopole
Asdex, dipole
AUG, monopole
AUG, dipole
0.00
0.05
0.10
0.15
n_H/n_e
0.20

(Fig. 5)

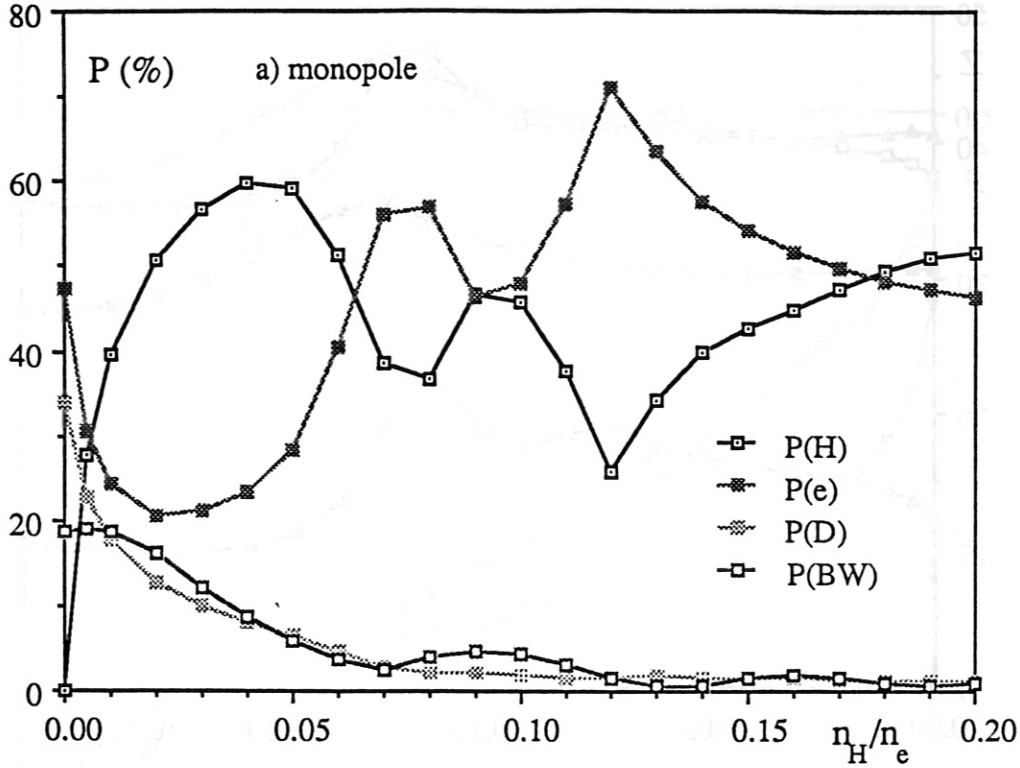
80
P (%)
a) monopole
60
40
20
0
P(H)
P(e)
P(D)
P(BW)
0.00
0.05
0.10
0.15
n_H/n_e
0.20

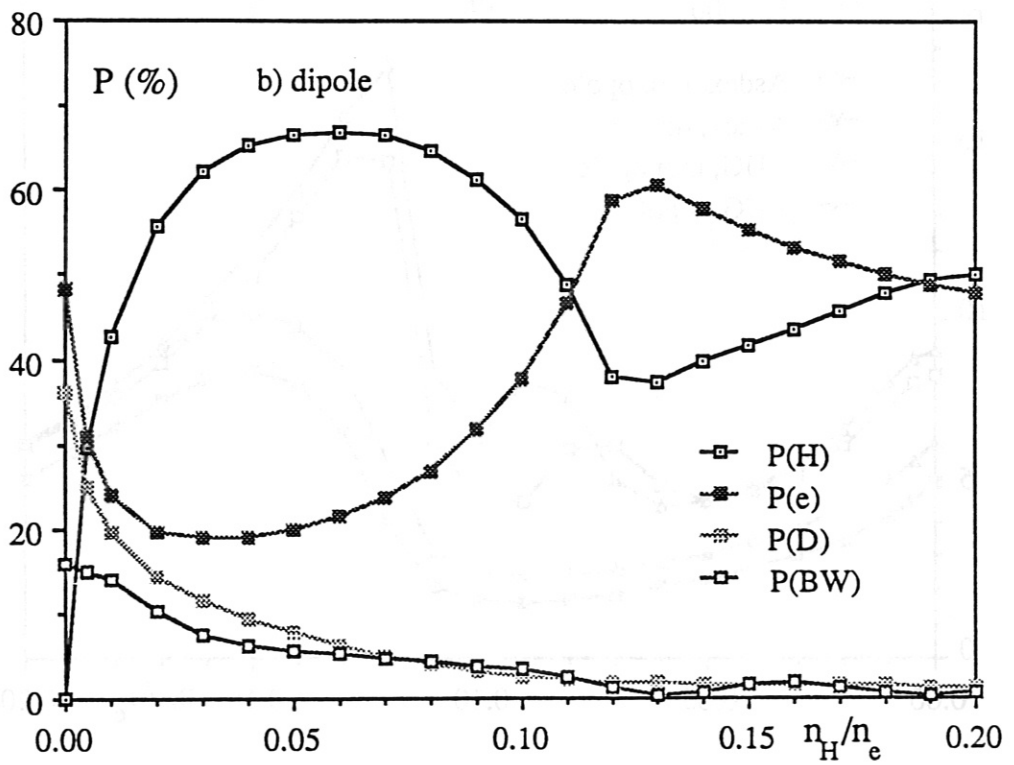
80
P (%)
b) dipole
60
40
20
0
P(H)
P(e)
P(D)
P(BW)
0.00
0.05
0.10
0.15
n_H/n_e
0.20

(Fig.6)

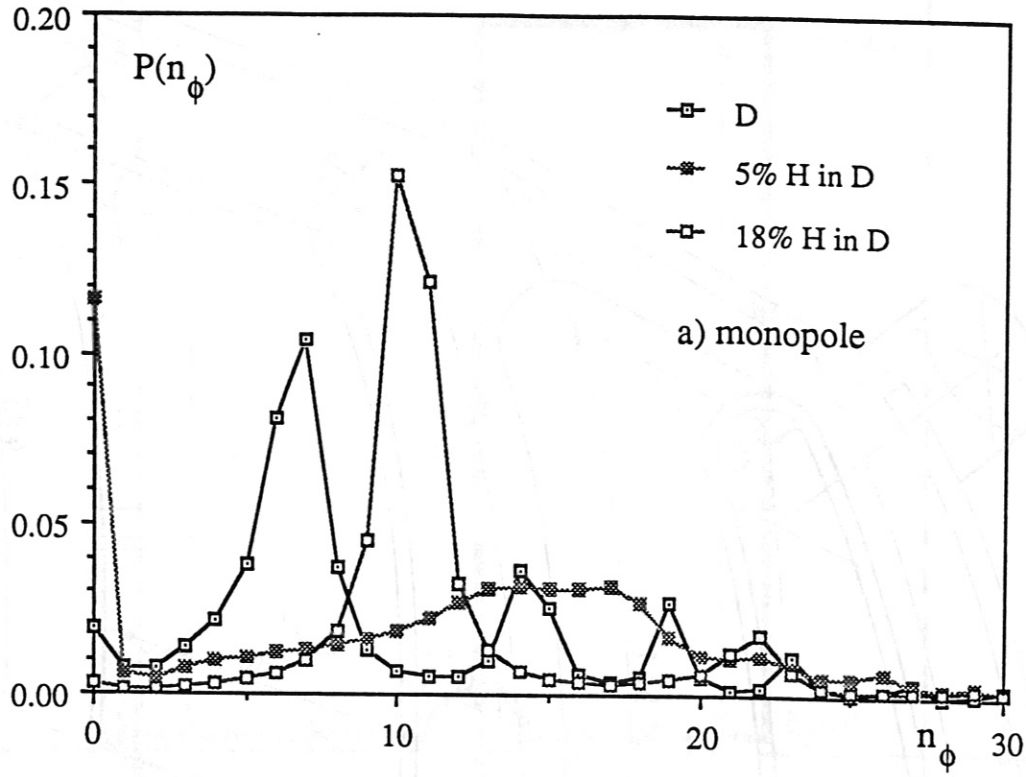
0.20
0.15
0.10
0.05
0.00
P(n$_\phi$)
D
5% H in D
18% H in D
a) monopole
0
10
20
n$_\phi$
30

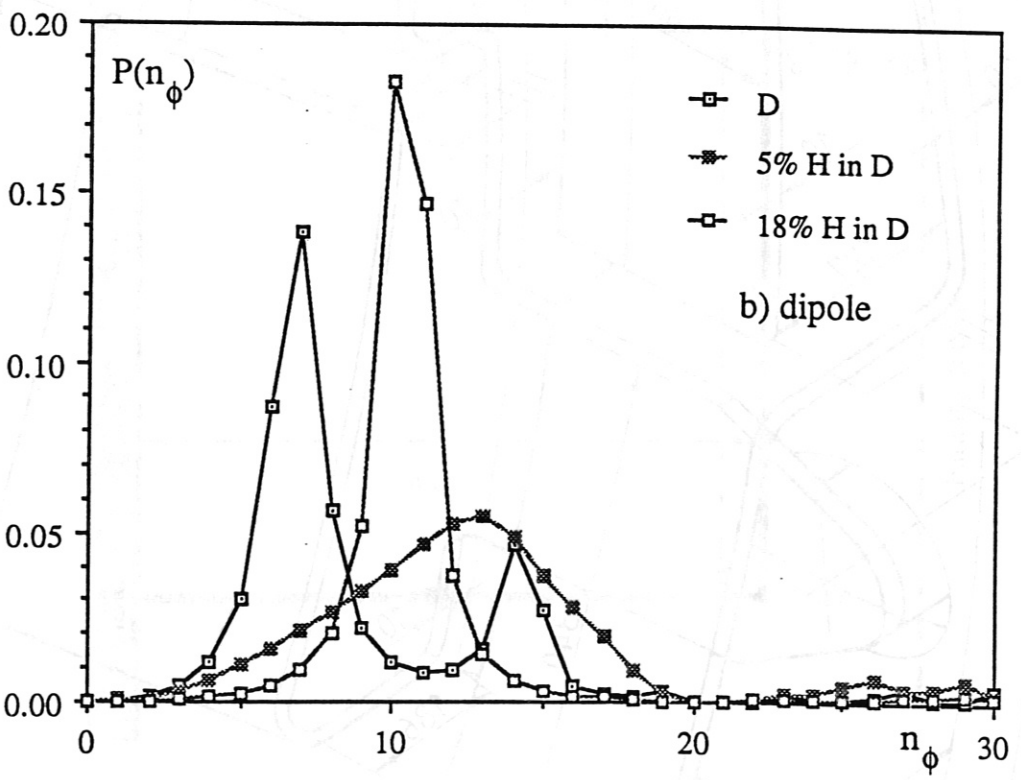
0.20
0.15
0.10
0.05
0.00
P(n$_\phi$)
D
5% H in D
18% H in D
b) dipole
0
10
20
n$_\phi$
30

(Fig.7)

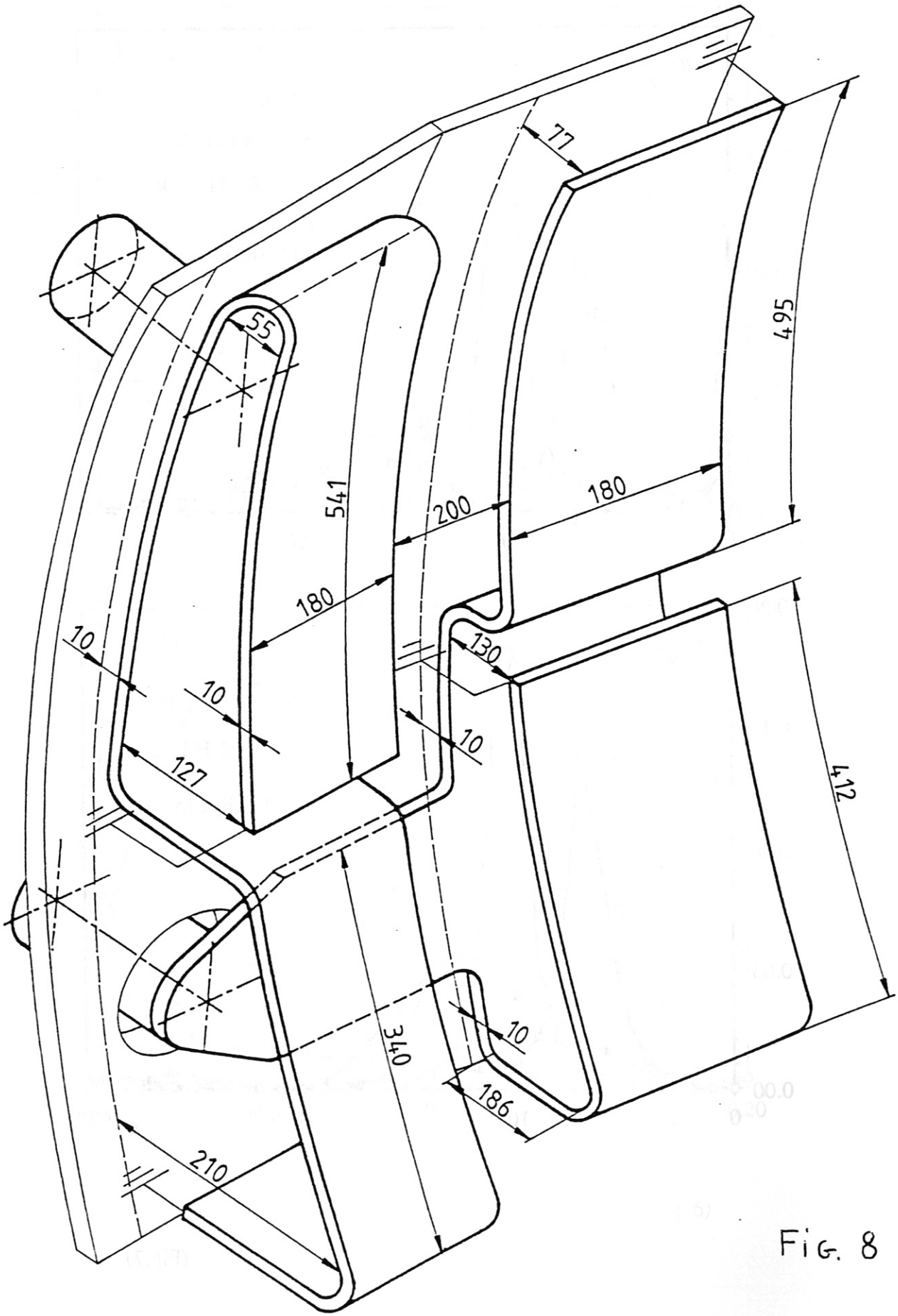

Fig. 8

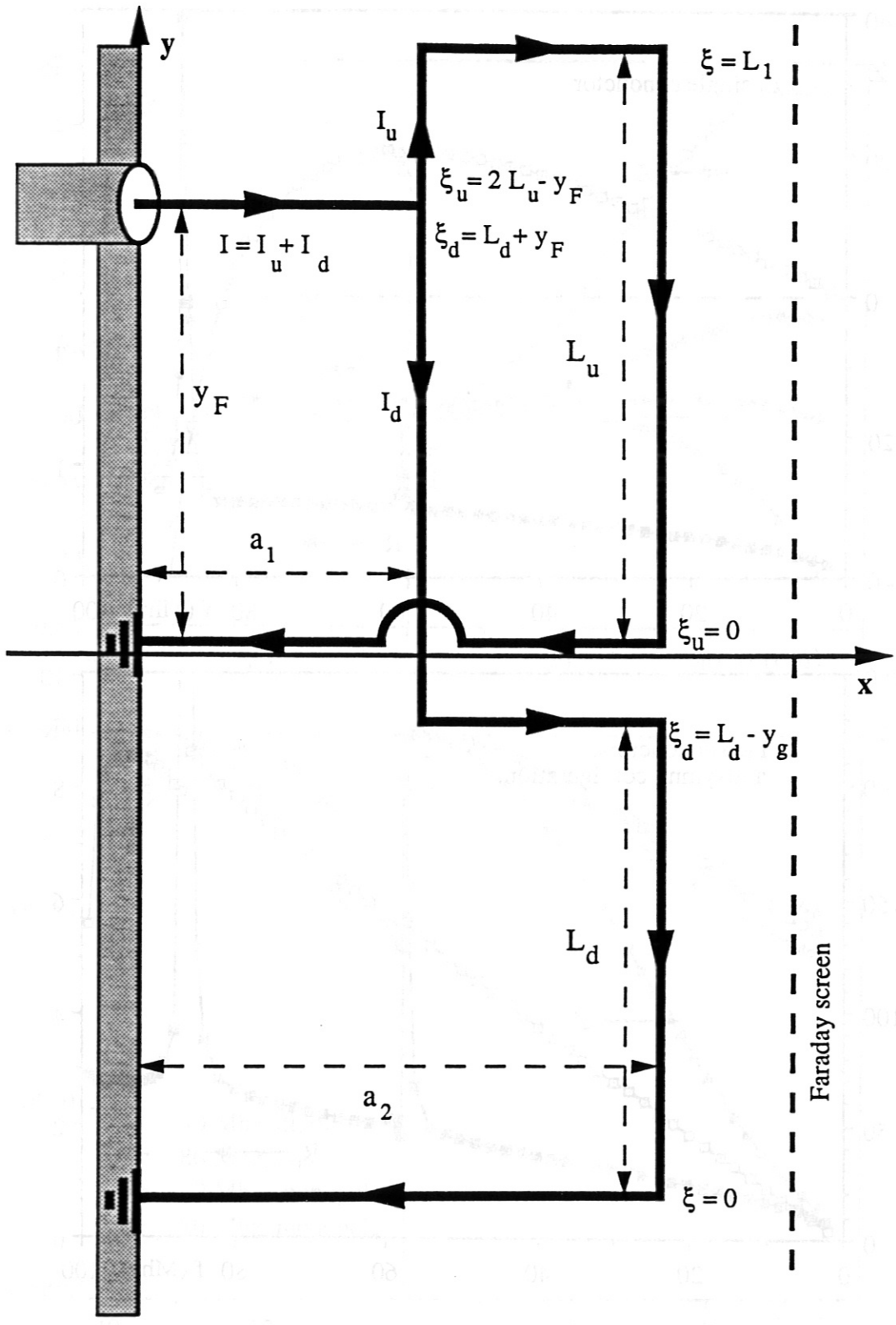
y
x
$\xi = L_1$
I_u
$\xi_u = 2L_u - y_F$
$\xi_d = L_d + y_F$
$I = I_u + I_d$
L_u
y_F
I_d
a_1
$\xi_u = 0$
$\xi_d = L_d - y_g$
L_d
a_2
$\xi = 0$
Faraday screen

(Fig.9)

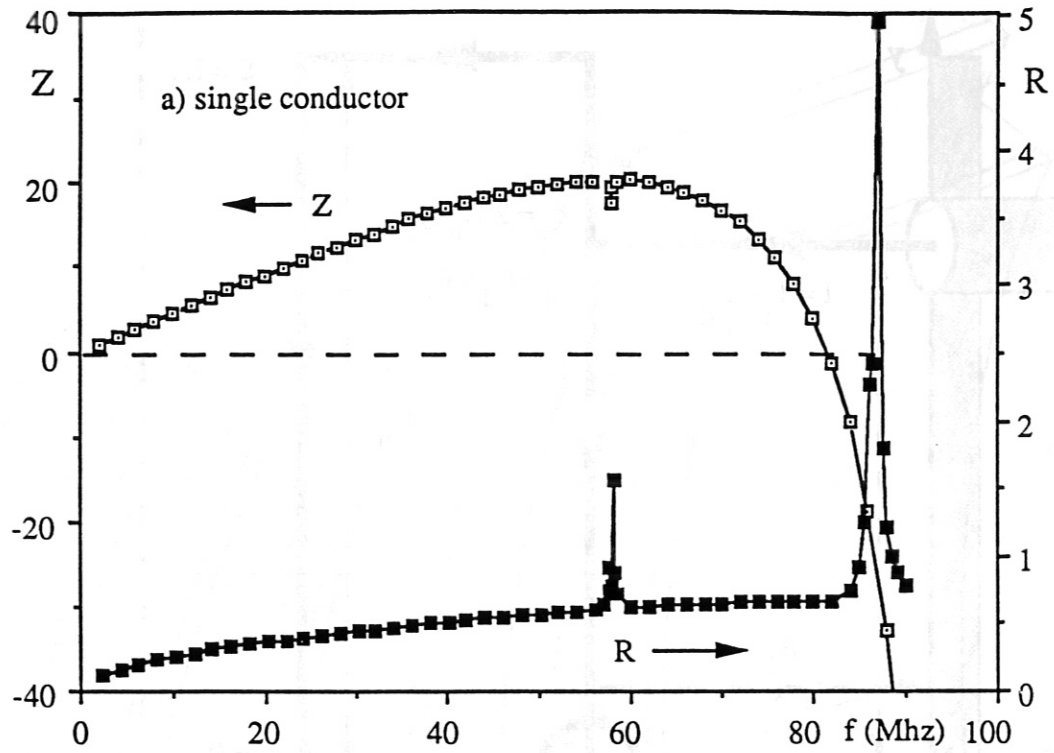
40
Z
20
0
-20
-40
5
R
4
3
2
1
0
a) single conductor
Z
R
0
20
40
60
80
f (Mhz)
100

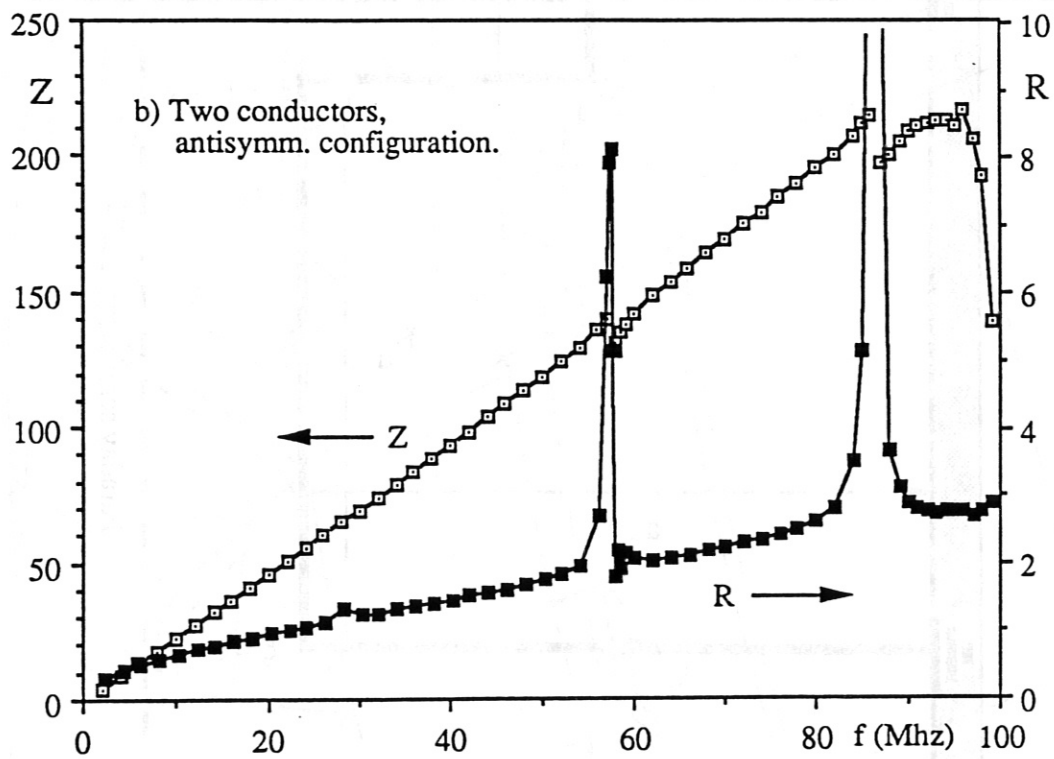
250
Z
200
150
100
50
0
10
R
8
6
4
2
0
b) Two conductors,
antisymm. configuration.
Z
R
0
20
40
60
80
f (Mhz)
100

(Fig.10)

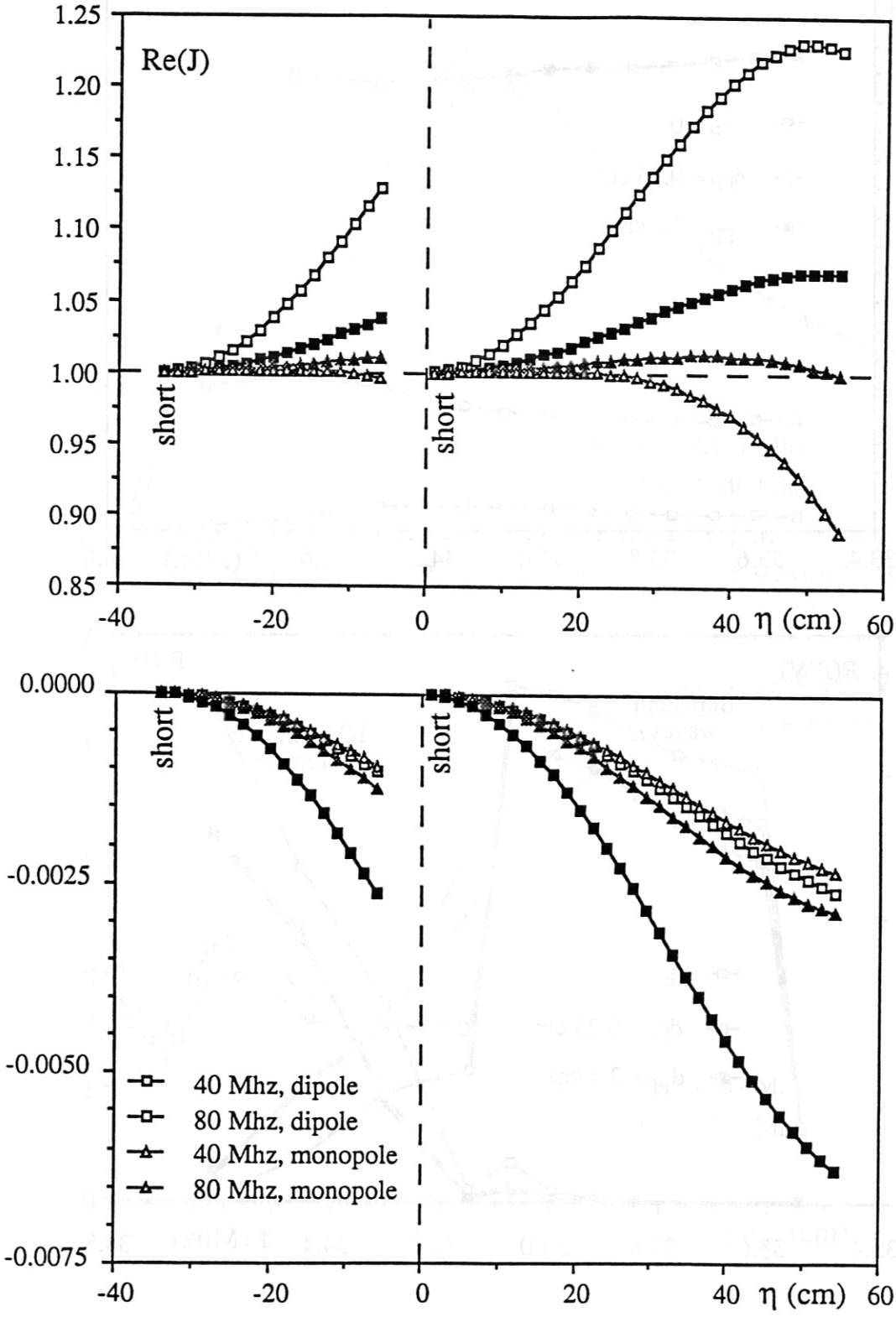
Re(J)
1.25
1.20
1.15
1.10
1.05
1.00
0.95
0.90
0.85
short
short
-40
-20
0
20
40
η (cm)
60
0.0000
-0.0025
-0.0050
-0.0075
short
short
40 Mhz, dipole
80 Mhz, dipole
40 Mhz, monopole
80 Mhz, monopole
-40
-20
0
20
40
η (cm)
60

(fig. 11)

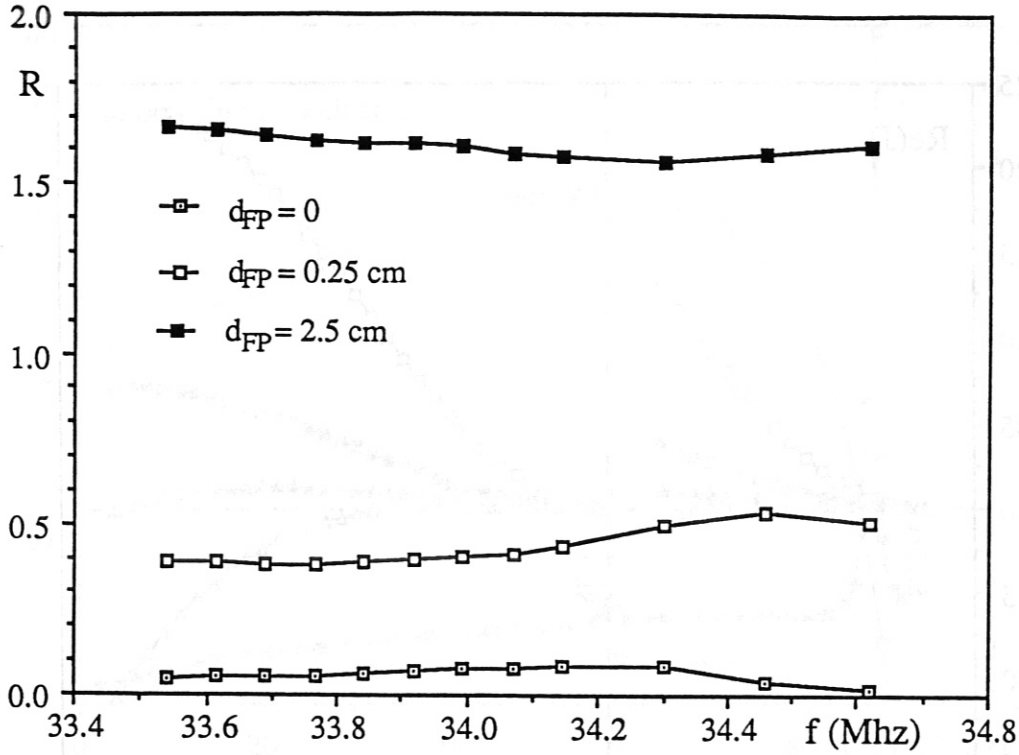
2.0
R
1.5
1.0
0.5
0.0
d_{FP} = 0
d_{FP} = 0.25 cm
d_{FP} = 2.5 cm
33.4
33.6
33.8
34.0
34.2
34.4
f (Mhz)
34.8

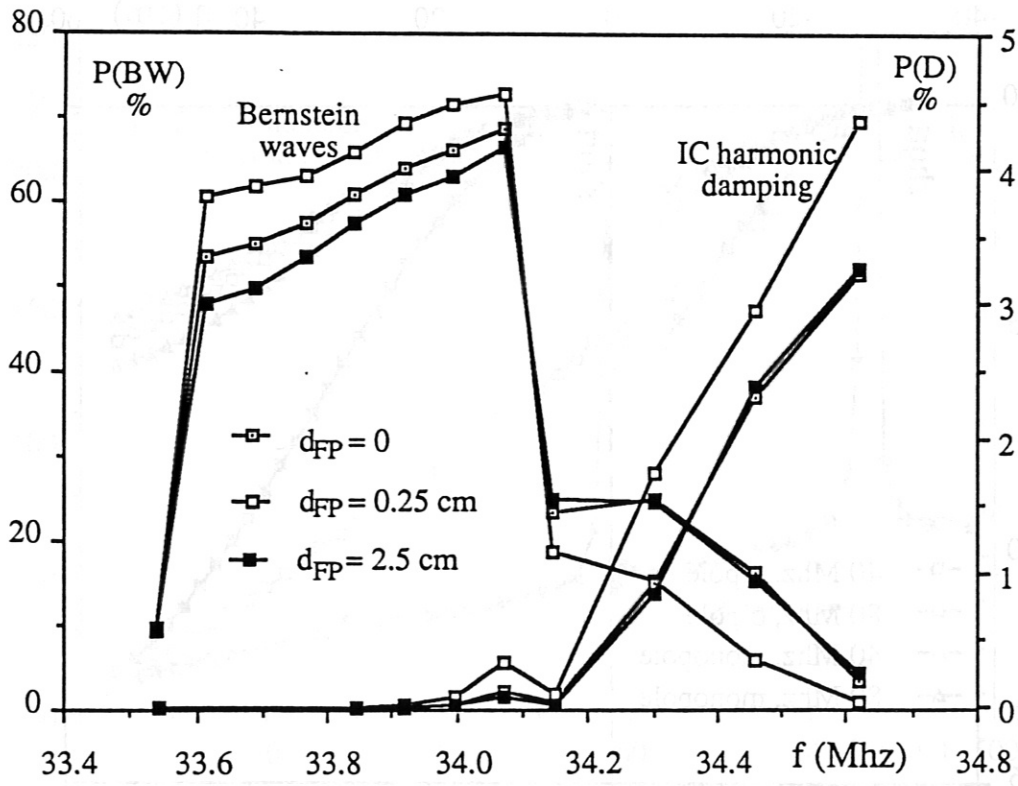
80
60
40
20
0
P(BW)
%
Bernstein
waves
P(D)
%
IC harmonic
damping
5
4
3
2
1
0
d_{FP} = 0
d_{FP} = 0.25 cm
d_{FP} = 2.5 cm
33.4
33.6
33.8
34.0
34.2
34.4
f (Mhz)
34.8

(Fig. 12)

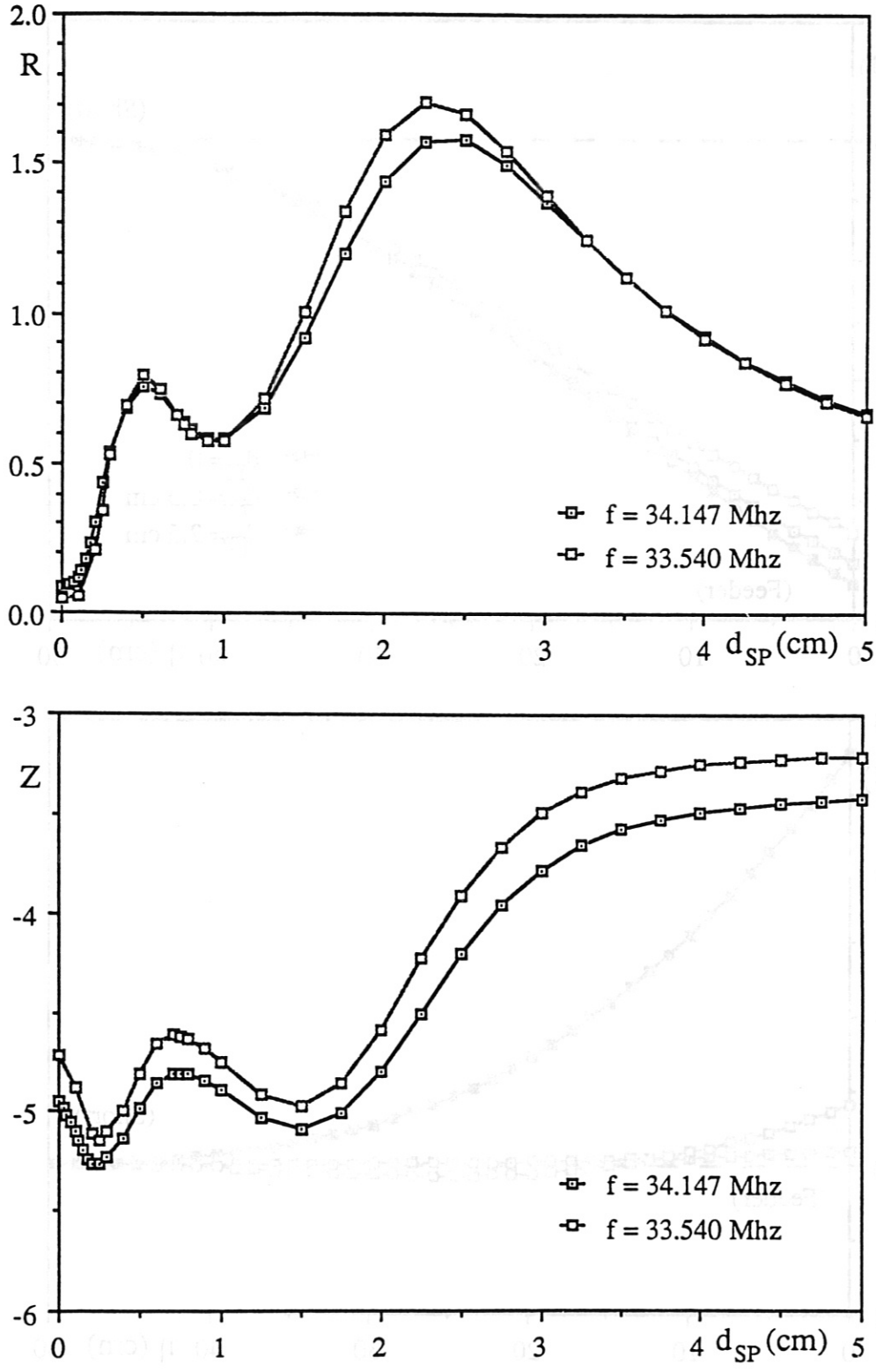
2.0
R
1.5
1.0
0.5
0.0
0
1
2
3
4
5
d_{SP}(cm)
f = 34.147 Mhz
f = 33.540 Mhz
-3
Z
-4
-5
-6
0
1
2
3
4
5
d_{SP}(cm)
f = 34.147 Mhz
f = 33.540 Mhz

(Fig. 13)

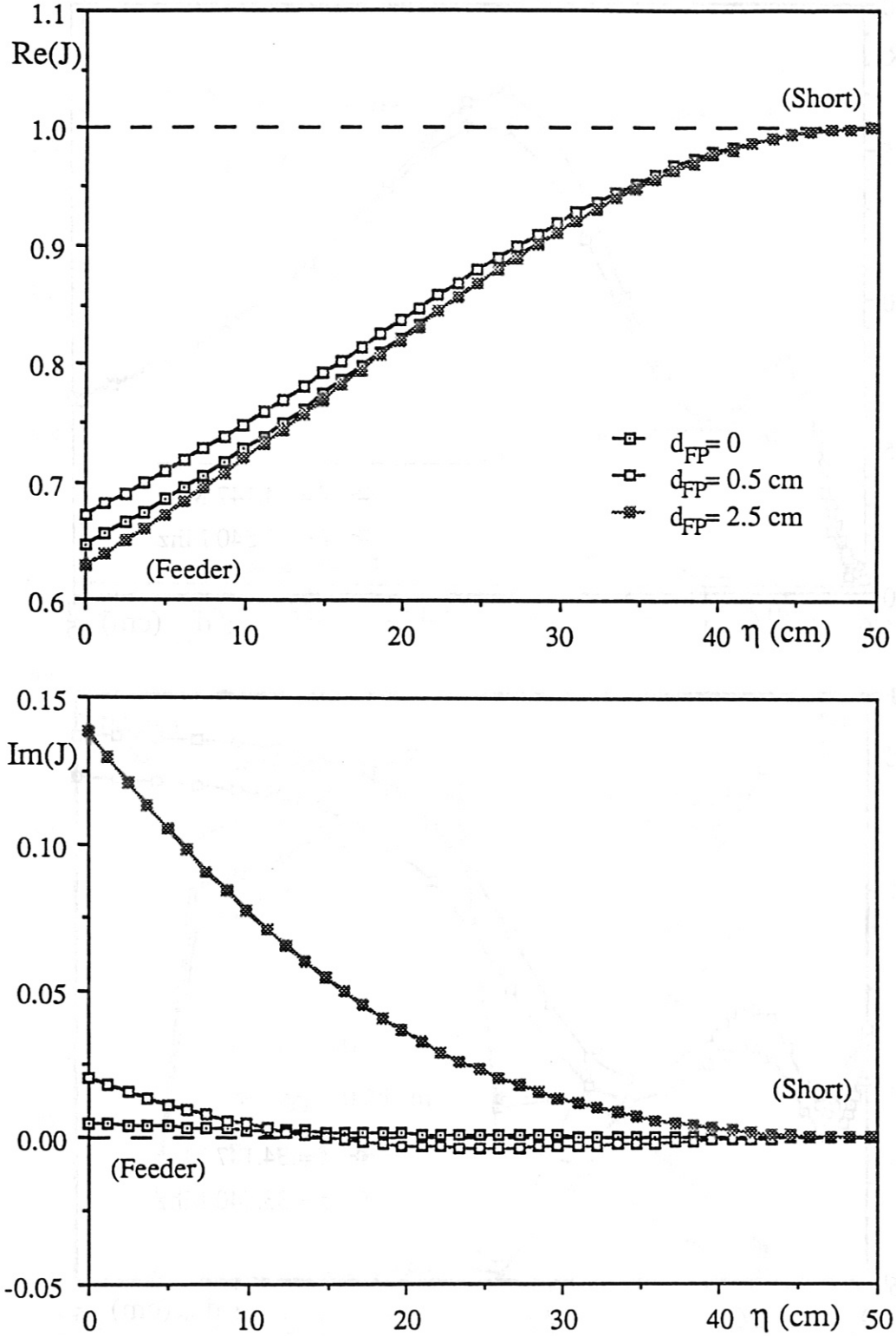
1.1
Re(J)
1.0
0.9
0.8
0.7
0.6
(Short)
(Feeder)
d_{FP}= 0
d_{FP}= 0.5 cm
d_{FP}= 2.5 cm
0
10
20
30
40
η (cm)
50
0.15
Im(J)
0.10
0.05
0.00
-0.05
(Short)
(Feeder)
0
10
20
30
40
η (cm)
50

(Fig. 14)